

Viscoelasticity of *in silico* Cytoskeletal Networks

A Thesis

Submitted to

Indian Institute of Science Education and Research Pune in partial
fulfilment of the requirements for the BS-MS Dual Degree Programme

by

Krishna Iyer V S



Indian Institute of Science Education and Research Pune
Dr. Homi Bhabha Road,
Pashan, Pune 411008, INDIA.

April, 2025
Supervisor: Prof. Dr. Stefan Klumpp
Krishna Iyer V S

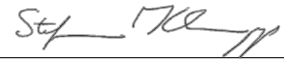
All Rights Reserved

Certificate

This is to certify that this dissertation entitled “Viscoelasticity of *in silico* Cytoskeletal Networks” towards the partial fulfilment of the BS-MS dual degree programme at the Indian Institute of Science Education and Research, Pune represents study/work carried out by Krishna Iyer V S at Georg-August University under the supervision of Prof. Dr. Stefan Klumpp, Professor, Institute for Dynamics of complex systems, during the academic year 2024-2025



Krishna Iyer V S



Prof. Dr. Stefan Klumpp

Declaration

I hereby declare that the matter embodied in the report entitled “Viscoelasticity of *in silico* Cytoskeletal Networks” are the results of the work carried out by me at the Department of Physics, Georg-August University, Göttingen, under the supervision of Prof. Dr. Stefan Klumpp and the same has not been submitted elsewhere for any other degree

A handwritten signature in black ink, reading "Krishna Iyer V S". The signature is written in a cursive style with a horizontal line underneath.

Krishna Iyer V S

Acknowledgements

I thank Dr. Yoav Pollack, Dr. Komal Bhattacharyya and Prof. Dr. Stefan Klumpp for their guidance and supervision during the project, Raffaele Mendoza, Dr. Serge Dimitrieff and Dorian Marx for their valuable discussions regarding the rheology of biopolymer networks and Dr. Vijayakumar Chikkadi for agreeing to be the expert for this project. I also thank my fellow labmates at the Theoretical Biophysics Group for providing an amazing and collaborative environment, and IISER for introducing me to a wonderful circle of friend. And of course, without the constant support from my parents for well over two decades, this thesis would not exist.

Finally, I would like to thank the Theoretical Biophysics Group and the CYTAC research training group for hosting me. I also acknowledge the funding support provided by the DFG (through RTG 2756) and KVPY for this project.

Contents

1	Introduction	15
1.1	The Cytoskeleton	15
1.2	Rheology	16
1.2.1	Viscoelasticity	16
1.2.2	The Complex Shear Modulus	17
1.2.3	Measuring Viscoelasticity	18
2	Methods	21
2.1	Cytosim	21
2.2	Extracting G^* from MSD	23
2.2.1	Theory	23
2.2.2	Mason’s method	24
2.2.3	Evans’ method	24
2.2.4	Segment Tracking Microrheology	25
2.3	Renewal Strategies	25
2.3.1	Cut and Paste (CnP) Renewal	25
2.3.2	Run and Tumble (RnT) Renewal	26
3	Results & Discussion	29
3.1	The Protocol	29
3.2	Bead Microrheology	30
3.3	Segment Tracking Microrheology	31
3.3.1	Using Segments as Probes	32
3.3.2	Tracking Segments and Modification	32
3.3.3	Matching benchmark simulation	33
3.4	Parameter scans	35
3.5	Introducing Renewal	38
3.5.1	Cut and Paste Renewal	38
3.5.2	Run and Tumble (RnT) renewal	39
3.6	Cytocalc	43

4	Conclusion	45
4.1	Summary	45
4.2	Outlook	46
4.2.1	Quantitative Matches with Experimental Results	46
4.2.2	Rheology Techniques	46
4.2.3	Renewal Models	46
4.2.4	Activity and Network Complexity	47
	Appendices	49
A	Derivations	51
A.1	The Generalized Stokes Einstein Relation	51
A.2	Crosslinker Binding Time	52
A.3	Renewal-Driven Cross-linker Unbinding	54
B	Additional Results	55
B.1	Bead Microrheology	55
B.1.1	Bead Size	55
B.1.2	Sanity Checks	55
B.1.3	Using Spheres	56
B.2	Frequencies, Times and Timesteps	57
B.2.1	Timestep and Equilibration	58
C	Technical Notes	61
C.1	Cytosim Configuration File	61
C.1.1	Using Templates	62
C.2	Reporting Random Filament Segment	62
C.3	Units in Cytosim	63
C.4	Cytosim on the Cluster	63
D	Miscellaneous Figures	65

List of Figures

1.1	Components of the Cytoskeleton	15
1.2	Maxwell's model for a Viscoelastic Material	17
1.3	Bulk Rheology: Stress response for oscillatory strain.	18
1.4	Microrheology Schematic	19
2.1	Cytosim: Fibers and Couples	22
2.2	Deletion-Creation Renewal Strategy	26
2.3	Two-State Model for filament renewal	26
2.4	Schematic: RnT (Run and Tumble) Renewal	27
3.1	MSD of Bead in Network	31
3.2	Viscous (G'') and Elastic (G') moduli extracted from bead MSD.	31
3.3	MSD and Shear Modulus for a free filament segment	32
3.4	MSD of Segment in Network	33
3.5	Effect of medium viscosity on G^*	34
3.6	Comparison with the benchmark	35
3.7	MSD: Varying Cross-linker Concentrations	35
3.8	G^* : Varying Cross-linker Concentrations	36
3.9	G and G' vs Cross-linkers	36
3.10	Creep (G''/G') vs ω	37
3.11	The tube model for cross-linked filament	38
3.12	Coarse Renewal Model: MSD	39
3.13	RnP Renewal: Filament length distributions	40
3.14	RnT Renewal: MSD	41
B.1	Bead Microrheology: Sanity Checks	56
B.2	Bead Microrheology: Using Spheres as a Probe	56
B.3	G^* extracted from stitched MSD	57
B.4	Storage modulus for different timesteps	58
B.5	Fraction of doubly bound cross-linkers vs time	59
D.1	Complex shear moduli with increasing number of crosslinkers.	65

D.2	Loss and Storage Moduli: Varying timesteps	65
D.3	Comparison: Mason’s Method vs Evans’ Method	65

List of Tables

3.1	Parameters of benchmark simulation, in Cytosim units. Fil:Filament, Cl:Cross-linker	30
C.1	Cytosim Units	63

Abstract

The cytoskeleton, a dynamic network of semiflexible filaments and associated proteins, plays a central role in maintaining cellular shape, organizing intracellular structures, and transmitting and generating mechanical forces. The viscoelastic properties of these networks govern their mechanical response, which has been extensively studied in cross-linked systems using computational and theoretical approaches. However, biological cytoskeletal networks—such as the actin cortex—exhibit additional complexity due to active processes, including motor-driven forces and actin filament turnover. This study aims to establish a systematic *in silico* framework using the Cytosim simulation suite to probe the viscoelasticity of cytoskeletal networks. Using microrheology techniques, we investigate how cross-linker density and filament renewal dynamics influence network rheology. Furthermore, we introduce `cytoCalc`, a python package enabling reproducible analysis of Cytosim simulations, to facilitate broader exploration of cytoskeletal mechanics across diverse experimental and theoretical contexts.

Chapter 1

Introduction

1.1 The Cytoskeleton

Cells, as complex biological entities, exhibit a wealth of physical phenomena. One fascinating process is that of cellular morphogenesis, which governs how cells adopt diverse shapes and sizes, and respond to mechanical stress. For example, some cells, such as Leucocytes (also known as White Blood Cells) simply lack a well-defined shape, allowing them to squeeze through tiny gaps between tissues—a process known as diapedesis. This ability to reorganize in response to external forces is underpinned by the cytoskeleton—a dynamic network of filaments that serves as the cell’s structural scaffold and regulates the mechanical response [1].

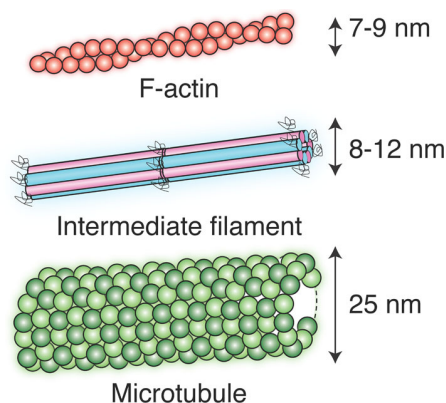


Figure 1.1: Actin, Microtubule and Intermediate Filaments [2]

The cytoskeleton consists of three classes of semi-flexible filaments—actins, microtubules and intermediate filaments (IFs)—and many associated proteins that cross-link, assemble, disassemble, or apply forces on these.

Actin Networks

Actin networks, in particular, play a central role in cellular force generation and shape determination. These networks, in association with cross-linking proteins such as α -actinin and myosin, exhibit interesting viscoelastic properties that have been extensively characterized both experimentally and theoretically.

Gittes *et al.* [3] performed computational and theoretical analysis of networks with passive cross-linkers and obtained a high-frequency power law for the frequency dependent complex

shear modulus (see Sec. 1.2.2) of $G^*(\omega) \sim \omega^{0.75}$, in line with experiments. Investigations by Broedersz *et al.* [4] on networks with dynamic cross-linkers established that, in the low frequency limit, the G^* follows a power-law behaviour $G \sim \omega^{\frac{1}{2}}$. Similarly, scaling regimes have been observed and characterized in entangled actin solutions [5, 6].

In addition to cross-linking, the constant turnover and treadmilling of actin can result in restructuring of the network, giving rise to non-trivial rheological properties. However, much less foray has been made into the study of renewal-dependent viscoelasticity of the cytoskeleton [7]. Similarly, recent experimental studies show that compound networks of actin and other Intermediate Filaments (such as vimentin) play an important role in determining the force response of cells [8]. The complexity of these networks makes them difficult to model, and since many computational studies of the cytoskeleton employ *in-house* modelling/simulations, the results are often not directly comparable.

In this project, we use Cytosim [9], an open source cytoskeleton simulation package, to measure the complex shear modulus ($G^*(\omega)$) of cross-linked actin networks and demonstrate that it captures known power law behaviours. As Cytosim is capable of modelling a wide variety of cytoskeletal features, this enables the study of dynamic, active and compound networks. In that vein, we present two models for renewal and study their effects on the physics of the network. Finally, we present a python package `cytoalc` as an accessible layer for quantifying rheology from Cytosim simulations, further facilitating the study of these networks by the scientific community.

1.2 Rheology

The previous section emphasized the importance of viscoelastic properties that cytoskeletal networks exhibit. For completeness, we present a brief look at the rheology (the study of mechanical response) of non-Newtonian materials, introducing physical quantities necessary for its characterization. For further reading, lecture notes from Pipkin [10] provides an intuitive picture for the various quantities defined herein.

1.2.1 Viscoelasticity

For a purely elastic material, the shear stress σ and the strain γ are related by Hooke's law:

$$\sigma(t) \propto \gamma(t) \implies \sigma(t) = G\gamma(t) \quad (1.1)$$

Similarly, Newton's law of viscosity relates the shear stress in a liquid to the strain rate:

$$\sigma(t) \propto \frac{d\gamma(t)}{dt} \implies \sigma(t) = \eta \frac{d\gamma(t)}{dt} \quad (1.2)$$

where G and η are the elastic modulus and the viscosity respectively. However, most real objects exhibit both elastic and viscous behaviour. Maxwell gave a simple representation of such materials by connecting an elastic spring in series to a ‘dashpot’ (a viscous liquid).

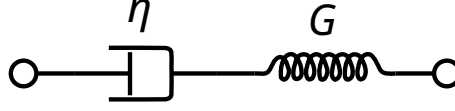


Figure 1.2: Maxwell's model for a Viscoelastic Material. CC0 Artwork from Wikipedia

Since the two components are connected in series, they experience the same stress $\sigma(t)$. Hence, the total strain is given by the sum of contributions from the spring and the dashpot:

$$\gamma_{\text{maxwell}}(t) = \frac{1}{G}\sigma(t) + \frac{1}{\eta} \int_0^t \sigma(t) dt \quad (1.3)$$

If stress is delivered in a very short ($t \ll \eta/G$) pulse, it is evident from Eq. 1.3 that the contribution from the viscous component would be negligible. Hence, the system behaves elastically, returning to its initial shape. However, upon application of a sustained stress, the viscous component dominates at long times, and the deformation no longer decays even if the stress is removed.

1.2.2 The Complex Shear Modulus

Suppose an oscillatory stress of the form $\mathcal{R}[Ae^{i\omega t}]$ is applied on the Maxwell solid. The strain response, from Eq. 1.3 would then be,

$$\begin{aligned} \gamma(t) &= \frac{1}{G}Ae^{i\omega t} + \frac{1}{i\omega\eta}Ae^{i\omega t} \\ &= \frac{G + i\omega\eta}{i\omega\eta G} \sigma(t) \end{aligned} \quad (1.4)$$

Rearranging the equation,

$$\begin{aligned} \sigma(t) &= \frac{i\omega\eta G}{G + i\omega\eta} \gamma(t) \\ &= \frac{G\omega^2\eta^2 + iG^2\omega\eta}{G^2 + \omega^2\eta^2} \gamma(t) \\ &= G^*(\omega)\gamma(t) = (G'(\omega) + iG''(\omega))\gamma(t) \end{aligned} \quad (1.5)$$

We define $G^*(\omega)$ as the frequency-dependent complex shear modulus or the ‘dynamic’ modulus, with G' and G'' being the elastic/storage modulus and the viscous/loss modulus

respectively.

Taking a derivative on both sides of Eq. 1.4, we can similarly define a complex viscosity $\eta^*(\omega)$, which is related to $G^*(\omega)$ by:

$$G^*(\omega) = i\omega\eta^*(\omega) \quad (1.6)$$

The Creep Compliance J

The compliance is a measure of ‘deformability’ of a material i.e the amount of shear produced by a unit stress. For elastic solids, it is the inverse of the shear modulus.

$$GJ = 1 \quad (1.7)$$

For viscoelastic materials, Eq. 1.7 is generalized using a convolution [11]:

$$\{G * J\}(t) = \int_0^t G(t')J(t-t')dt' = t \quad (1.8)$$

Using the convolution theorem¹ ($G^*(\omega)J^*(\omega) = \mathcal{F}_u(\{G * J\}(t))$) where \mathcal{F}_u is the unilateral Fourier transform, we obtain a relation between the complex shear modulus and the complex creep compliance:

$$G^*(\omega)J^*(\omega) = \frac{1}{i\omega} \quad (1.9)$$

1.2.3 Measuring Viscoelasticity

Bulk Rheology

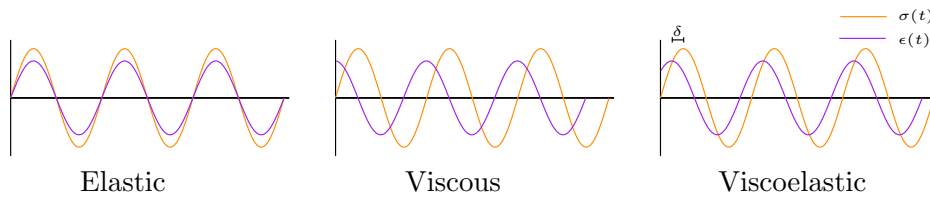


Figure 1.3: Bulk Rheology: Stress response for oscillatory strain.

Building upon the theoretical framework of viscoelasticity outlined in Sec. 1.2.2, bulk rheology offers a direct experimental approach to quantify the frequency-dependent complex shear modulus ($G^*(\omega)$). This method involves applying a controlled oscillatory shear strain ($\gamma(t) = \gamma_0 e^{i\omega t}$) to the material and measuring the resultant stress response ($\sigma(t)$).

¹The time derivative arises since $G^*(\omega)$ (as defined in Sec. 1.2.2) actually represents the Fourier transform of the time derivative of $G(t)$ - and we use the property $\{\dot{u} * v\} = \{i\omega u * v\}$

By analyzing the amplitude ratio and phase lag (δ) between the applied strain and measured stress, the elastic (storage) modulus ($G'(\omega)$) and viscous (loss) modulus ($G''(\omega)$) can be obtained:

$$G' = \frac{\sigma_0}{\gamma_0} \cos(\delta)$$

$$G'' = \frac{\sigma_0}{\gamma_0} \sin(\delta)$$

Microrheology

In contrast to bulk rheology, microrheology offers an approach to characterize $G^*(\omega)$ by analyzing the motion of probes embedded within the material. In *passive* microrheology, the thermal fluctuations of the probe is used as a proxy for viscoelasticity, relating their mean-squared displacement (MSD) to the material's response via the generalized Stokes-Einstein relation (GSER) as depicted in the schematic in Fig. 1.4. In *active* microrheology, controlled external forces (e.g., via optical tweezers or magnetic fields) are applied on the probe, enabling direct measurement of frequency-dependent compliance.

From an experimental standpoint, these techniques provide the means to characterize a material without causing structural damage due to shearing, or to study spatial variation in a heterogeneous environment. In simulations both approaches are typically feasible, and the choice often reduces to technical considerations or to whether one attempts to emulate experiments. In Sec. 2.2, we discuss the theoretical and practical framework of employing passive microrheology.

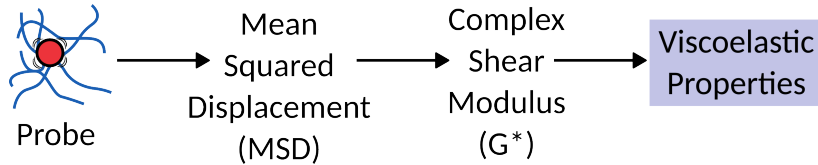


Figure 1.4: Bead Microrheology Schematic

Chapter 2

Methods

2.1 Cytosim

Cytosim is an extensible, agent-based stochastic dynamics simulation suite developed by Nedelec *et al.* [9] for modelling semi-flexible filament networks and associated molecular components. Cytosim provides implementations for ‘high-level’ objects, such as fibers, beads and couples, which can be added to a simulation using a straightforward syntax. For example, the following code initializes 500 actin-like fibers with specified mechanical properties:

```
set fiber actin {  
    rigidity      = 0.1  
    steric        = 1, 0.0035  
    segmentation = 0.0028  
}  
new 500 actin { length = 1.5 }
```

A full configuration file (corresponding to the system described in Sec. 3.3.3) is included in Appendix Sec. C.1. These objects are represented by points, stored in an $N \times d$ array \mathbf{x} , where N is the number of points and d the dimensionality of the system. The dynamics of the points is governed by an overdamped Langevin equation,

$$d\mathbf{x} = \mu \mathbf{F}(\mathbf{x}, t) dt + d\mathbf{B}(t) \quad (2.1)$$

$\mathbf{F}(\mathbf{x}, t)$ is an $N \times d$ array of forces acting on the points and $\mathbf{B}(t)$ is a stochastic noise term that gives rise to Brownian motion. The mobility, μ , is calculated using a ‘drag model’ specific to its shape. After an implicit integration scheme is used to solve Eq. 2.1, additional constraints (such as for keeping filament lengths fixed) are satisfied using Lagrange multipliers [9].

Given the central role of fibers and couples in this project, a short description of each object

type, with some implementation details, has been provided below.

Fibers

Cytosim models a **Fiber** as a semi-flexible, piecewise-linear chain of N vertices with additional constraints ensuring that the distance between consecutive vertices remains constant¹. Each fibre has a radius given by the steric range (r_s), within which other objects experience a force:

$$F = k_s(r_b - d) \quad \begin{cases} d = \text{distance from the centre of the filament} \\ k_s = \text{Stiffness Coefficient} \end{cases}$$

Fibers can dynamically grow and shrink (both from the **Plus end** and the **Minus end**) at specified rates. The number of vertices of a dynamic filament is changed as required to maintain the segmentation length.

Couples

A **Couple** is a composite object containing two **hands** connected by a spring of stiffness k and zero resting length. When within binding range r_b of a filament, a hand binds to it at a rate κ_b . Unbinding events happen at a rate κ_{ub} , or if the force on the couple exceeds some threshold f_T . In our simulations, κ_{ub} and f_T were set to 0 and infinity respectively to match the benchmark simulation, corresponding to no unbinding.

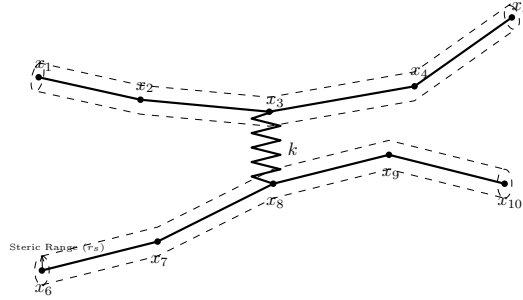


Figure 2.1: Fibers and Couples in Cytosim. The points x_i represent the vertices of filaments, constrained such that $|x_i - x_{i+1}|$ is constant. A couple with spring constant k cross-links the two filaments. Figure adapted from Nedelec *et. al.* (2007) [9]

Couples can be used to emulate molecular motors or cross-linkers depending on the **activity** of the hand. With hands that can only *bind*, the couples used in Sec. 3.1 act as fixed cross-linkers.

¹and roughly equal to a specified segmentation length l_s . Since the total length of the filament can be specified independently of l_s , it need not be an integral multiple of l_s . Cytosim adjusts the actual length of each segment such that the absolute difference between the *true* and *expected* (l_s) segment lengths is minimized

2.2 Extracting G^* from MSD

In a Newtonian fluid, a particle's diffusivity is related to the viscosity of the medium by the Stokes-Einstein relation.

$$D = \frac{k_B T}{6\pi\eta a} \quad (2.2)$$

This, however, is not directly applicable for systems that exhibit frequency dependent viscous behaviour—such as non-Newtonian fluids (Sec. 1.2.1). To address this limitation, Mason *et al.* [12] proposed a generalization of the Stokes-Einstein relation (GSER) for frequency dependent viscosities. In this section, we describe the generalization and, in some detail, discuss the algorithms we use to extract the complex shear modulus.

2.2.1 Theory

Before introducing the generalized equation, let us look at a 3-dimensional particle of radius a in a purely viscous fluid. The mean squared displacement for this particle given by [13]:

$$\langle \Delta r^2(t) \rangle = 6Dt = \frac{k_B T t}{\pi\eta a} \quad (2.3)$$

While $\langle \Delta r^2 \rangle$ is typically described as a function of time, we can, in principle, apply a unilateral Fourier transform [14] on Eqn. 2.3 to obtain a frequency dependent mean-squared displacement.

$$\langle \Delta r^2(\omega) \rangle = -\frac{k_B T}{\pi\eta\omega^2 a} \quad (2.4)$$

where $\langle \Delta r^2(\omega) \rangle$ is the MSD in Fourier space.

The Generalized Stokes-Einstein Relation similarly relates the $\langle \Delta r^2(\omega) \rangle$ of a particle in a non-Newtonian liquid to a frequency dependent viscosity $\eta^*(\omega)$:

$$\langle \Delta r^2(\omega) \rangle = -\frac{k_B T}{\pi\eta^*(\omega)\omega^2 a} \quad (2.5)$$

From Eq. 2.5 and Eq. 2.4, it is evident that the standard Stokes-Einstein relation is retrieved from the GSER for a medium with frequency-independent viscosity η . Appendix Sec. A.1 presents a rigorous derivation of Eq. 2.5 starting from a generalized Langevin equation.

Substituting $G^*(\omega) = i\omega\eta^*(\omega)$ in Eq. 2.5 and rearranging,

$$G^*(\omega) = \frac{k_B T}{i\pi\omega a \langle \Delta r^2(\omega) \rangle} = \frac{k_B T}{i\pi\omega a \mathcal{F}_u\{\langle \Delta r^2(t) \rangle\}} \quad (2.6)$$

In Eq. 2.6, we have a theoretical framework for extracting the complex shear modulus $G^*(\omega)$ from the Fourier transform (\mathcal{F}_u) of the mean squared displacement. In addition to Eq. 2.6, the GSER is often be represented using other quantities [15]. For example, in Sec. 2.2.3, we use a version that relates the creep compliance $J(t)$ to the mean-squared displacement:

$$\frac{\pi a}{k_B T} \langle \Delta r^2(t) \rangle = \frac{k_B T}{\pi a} J(t) \quad (2.7)$$

2.2.2 Mason's method

Using the Generalized Stokes-Einstein Relation to calculate the shear moduli requires performing a unilateral Fourier transform on an arbitrary MSD obtained from the simulation—or experiments. Since this is not always tractable, Mason *et al.* [14] use an estimate for the Fourier transform by expanding $\mathcal{F}_u\{\langle \Delta r^2(t) \rangle\}$ around $1/\omega$:

$$i\omega \mathcal{F}_u\{\langle \Delta r^2(t) \rangle\} \approx \langle \Delta r^2(1/\omega) \rangle \Gamma[1 + \alpha(\omega)] i^{-\alpha(\omega)} \quad (2.8)$$

Where $\Gamma[1 + \alpha]$ is the Gamma function and $\alpha(\omega)$ is defined as:

$$\alpha(\omega) = \left[\frac{d \ln \langle \Delta r^2(t) \rangle}{d \ln t} \right]_{t=1/\omega} \quad (2.9)$$

Using this approximation in Eq. 2.6, we get expressions for the Storage (G') and Loss (G'') moduli.

$$G'(\omega) = |G^*(\omega)| \cos(\pi\alpha(\omega)/2)$$

$$G''(\omega) = |G^*(\omega)| \sin(\pi\alpha(\omega)/2)$$

where $|G^*(\omega)|$ is given by:

$$|G^*(\omega)| \approx \frac{k_B T}{\pi a \langle \Delta r^2(1/\omega) \rangle \Gamma[1 + \alpha(\omega)]} \quad (2.10)$$

2.2.3 Evans' method

While Eq. 2.10 is a straightforward technique to obtain the frequency-dependent shear moduli, the approximate Fourier (or Laplace) transforms may affect the accuracy of the result. Evans *et al.* [11] devised an improved algorithm that sidesteps this by exploiting a property of the time dependent creep compliance $J(t)$ (defined in Sec. 1.2.2):

It is known that, for any material (viscous or viscoelastic), $J(t)$ at long time approaches a straight line. As a result, the double derivative of $J(t)$ has to vanish. Moreover, causality requires that $J(t)$ (and hence \ddot{J}) be 0 for time $t < 0$ [11]. As a result, the Fourier transform of \ddot{J} does converge under all conditions, and can be used to reconstruct the $\mathcal{F}_u[J](\omega)$:

$$\mathcal{F}_u[J](\omega) = \tilde{J}(\omega) = \frac{-1}{\omega^2} \mathcal{F}_u[\ddot{J}](\omega) \quad (2.11)$$

In practice, we perform a Discrete Time Fourier Transform (DTFT) [16] on $\ddot{J}(t)$ to find $\tilde{J}(\omega)$. Given $\tilde{J}(\omega)$, $G^*(\omega)$ is trivially calculated using,

$$G^*(\omega) = \frac{1}{i\omega\tilde{J}(\omega)} \quad (2.12)$$

2.2.4 Segment Tracking Microrheology

Sec. 2.2.1 describes the GSER for a spherical probe. To analyze our simulations, we also employ Segment Tracking Microrheology (STM), a technique devised by Kim *et al.* [17], where filament segments are use as the probe instead of beads. This requires adapting Equations Eq. 2.10 and Eq. 2.11 for cylindrical probes. This is achieved by replacing the radius of the bead a by an effective radius r_b that satisfies the following relation:

$$\zeta_{\perp} = 6\pi\eta_M r_b \quad (2.13)$$

where,

$$\zeta_{\perp} = 3\pi\eta_M\sigma \cdot \frac{3+2L/\sigma}{5} \quad (2.14)$$

is the transverse frictional coefficient of the segment (σ and L being the diameter—steric range in Cytosim—and length of the segment, respectively) and η_M is the viscosity of the medium.

2.3 Renewal Strategies

As mentioned in Sec. 1.1, the turnover and treadmilling of actin entails significant effects on the viscoelastic properties of the network. In this section, we discuss some implementations for filament renewal in Cytosim.

2.3.1 Cut and Paste (CnP) Renewal

This first implementation is based on a minimal model for renewal of filaments used by Belmonte *et al.* [18] to demonstrate pulsing in contracting actin networks. In this strategy,

filaments are randomly deleted (at a specified rate) and added back at a random location (Fig. 2.2).

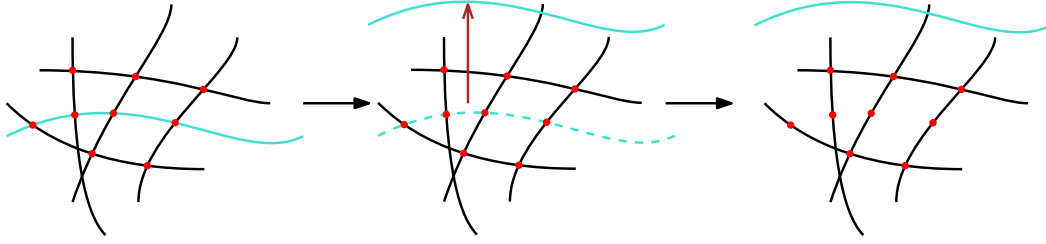


Figure 2.2: Deletion-Creation Renewal Strategy. Figure provided kindly by Dr. Yoav Pollock

However, when used in conjunction with STM, this poses a problem—the MSD of a filament segment is valid only for times between a creation and a deletion event. This reduces the total duration over which MSD is measured, which in turn shortens the frequency range of G^* . To overcome this limitation, we added ‘Probe filaments’ that do not renew and tracked only their MSD.

2.3.2 Run and Tumble (RnT) Renewal

While CnP renewal is efficient and easy to implement, a more realistic renewal model would incorporate renewal as changes in filament lengths, mimicking polymerization and depolymerization. First, we present a simple model that maintains an average filament length and discuss some of its limitations.

Consider a two state model of a filament with a ‘growing’ and a ‘shrinking’ state. Each filament flips from one state to another at a rate α .

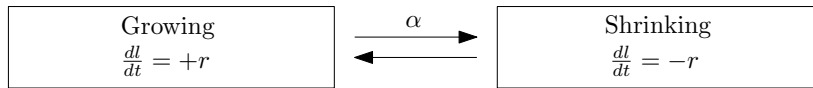


Figure 2.3: Two-State Model for filament renewal

This set of equations is reminiscent of 1-Dimensional Run and Tumble motion (Fig. 2.4). As a result, the dynamics of the length of a filament is well described by a RnT particle starting at $x_0 = l_0$, with a speed $v = r^2$. Since the mean position of a RnT particle is x_0 [19], we do not expect the average length of the filaments to change.

²Technically, since filament lengths are necessarily positive, the origin acts as an absorbing boundary. However, for small enough times ($t < l_0/v$) the dynamics is exactly described by an RnT particle

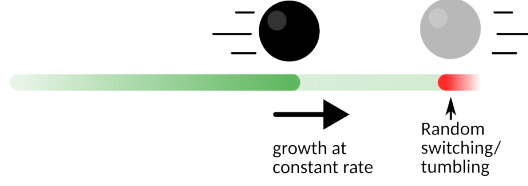


Figure 2.4: Schematic: RnT (Run and Tumble) Renewal

However, it is known that the probability distribution, $\psi(x, t)$, of a RnT particle does not have a steady state distribution, but rather follows [19]:

$$\langle x(t)^2 \rangle \approx 2D_{\text{eff}}t \quad D_{\text{eff}} = \frac{v^2}{2\alpha} \quad (2.15)$$

Therefore, the length distribution of the filaments with the two-state model would keep widening. Inside cells, however, the actin filament length distribution is highly regulated [20, 21]. Moreover, since the number of filaments is finite, the growing length distribution will result in a change in the mean length of filaments, contrary to our initial expectations. In order to overcome these issues, the model needs to be capable of constraining the length of the filaments to some finite domain.

Length Dependent Renewal

Theoretical work on generalized RnT particles suggests that using an inhomogeneous (position dependent) switching rates can trap a particle [22]. Singh *et al.* [23] showed that employing two step functions, as defined in Eq. 2.16, it is possible to limit length fluctuations.

$$\alpha_{g \rightarrow s} = \begin{cases} \alpha & l > l_{\text{high}}, \\ 0 & \text{otherwise} \end{cases} \quad \alpha_{s \rightarrow g} = \begin{cases} r & l < l_{\text{low}}, \\ 0 & \text{otherwise} \end{cases} \quad (2.16)$$

Chapter 3

Results & Discussion

In this section, we present the results of our investigation, commencing with the benchmarking of our microrheological framework against established computational studies by Kim *et al.* [17]. Subsequently, we explore the influence of cross-linking density on network rheology, quantifying transitions from viscous to elastic behaviour. Building on this, we introduce dynamic filament renewal models to probe the mechanical consequences of turnover processes, providing a preliminary framework for future studies of renewing cytoskeletal networks. Finally, we present *cytoalc*, a python package designed to enhance reproducibility and extensibility of Cytosim-based rheological studies, facilitating broader exploration of cytoskeletal mechanics across diverse experimental and theoretical contexts.

3.1 The Protocol

We prepare a cross-linked network of actin-like filaments in Cytosim (Sec. 2.1), adapting parameters from Kim *et al.* [17]. Table 3.1 lists the common parameters used in the simulations, expressed in Cytosim units (c.u.). A cubic box of side length $2.8 \mu\text{m}$ with periodic boundary conditions (PBC) is initialized with 500 filaments. In case of bead microrheology, a $0.3 \mu\text{m}$ bead (probe) is added at the centre of the box. After a short equilibration¹ of 5s cross-linkers are added, and the system is equilibrated for 50s. Both the timestep and the equilibration time are chosen according to the discussion in Sec. B.2.1.

The highest frequency our $G^*(\omega)$ is valid for is determined by the frame-rate² and the lowest by the total duration of the simulation (Appendix Sec. B.2). However, running long simulations at high frame-rates, the amount of data produced increases exponentially with each additional decade in frequency.

¹Filaments are randomly placed without any bending. This short equilibration imparts Brownian fluctuations onto the segments

²This is the reciprocal of the time between two saved frames (t_f) which is often longer than the *timestep*

To avoid this, different simulations are run for different ranges of frequency with a reasonable balance between duration and framerate. For example, we use post-equilibration durations of 5s (high frame-rate), 50s, and 500s (longer durations), saving 500 regularly spaced frames in each case. With this setup, the data storage requirements grow linearly with the number of decades in frequency. In Appendix Sec. B.2, we also explored, with little success, the idea of ‘stitching’ the MSD from the three simulations and extracting the shear modulus from a single, long-time, high frame-rate MSD.

Parameter	Value
Timestep	0.0001
Box Length	2.8
Periodicity	xyz
Viscosity	0.1
Fil. length	1.5
Fil. rigidity	0.001
Fil. Segmentation	0.07
Fil. Steric Range	0.007
Fil. Steric Force	16.9
Cl. Binding Rate	10
Cl. Binding Range	0.02
Cl. Unbinding Rate	0
Cl. Stiffness	4.23
Cl. Diffusion	10

To obtain ensemble-averaged measurements, we ran 80 trials for each system configuration. These were run in big batches on the Göttingen university physics department’s rocks computing cluster

Table 3.1: Parameters of benchmark simulation, in Cytosim units.

Fil:Filament, Cl:Cross-linker

(Appendix Sec. C.4). For bead probes, the MSD is averaged across all the simulations (each containing a single bead). With filament probes, as in the case of Segment Tracking Microrheology (STM), random filament segments (one per filament) (Appendix Sec. C.2) were tracked as probes, with the MSD averaged over all probes across all trials.

3.2 Bead Microrheology

To mimic experimental conditions, a $0.3 \mu\text{m}$ bead was inserted into the system, and its MSD was measured. The bead size was selected based on the network’s mesh size (Appendix Sec. B.1.1). For viscoelastic systems, the MSD typically exhibits subdiffusive power-law scaling. However, while the diffusion constant was reduced to two-thirds of the expected value for a free viscous bead (Fig. 3.1 (Left)), the MSD remained diffusive (Fig. 3.1 (Right)), with slopes of 1 in log-log plots.

The extracted G^* (Fig. 3.2) showed no elastic component (G' fluctuating around 0), while G'' increased linearly with frequency—a signature of purely viscous systems (Sec. 1.2.2), consistent with the slope of the MSD. Despite expectations that cross-linkers would induce elasticity [24], increasing their numbers had no observable effect (Fig. 3.1).

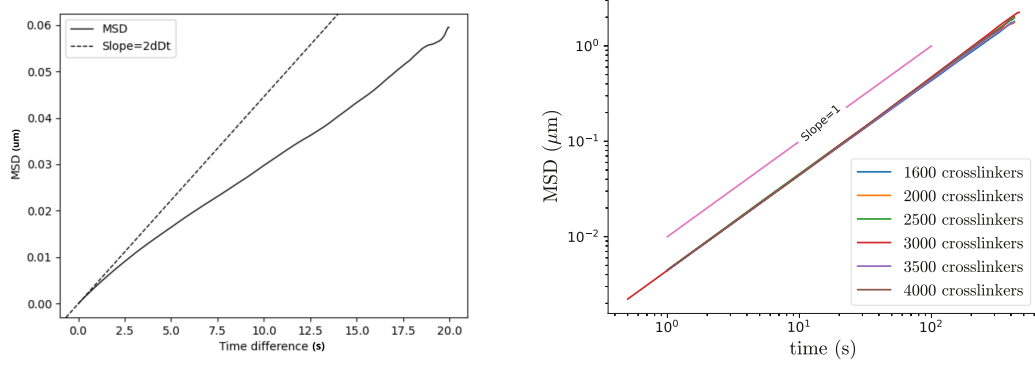


Figure 3.1: (Left) MSD of probe in the network (linear scale). The dotted line shows the theoretical MSD of a probe of the same radius in a purely viscous medium (with viscosity from table 3.1). (Right) MSD of probes in log-log scale for various cross-linker counts. The slope of the curves is 1, indicating purely diffusive behaviour ($\text{MSD} \propto t$)

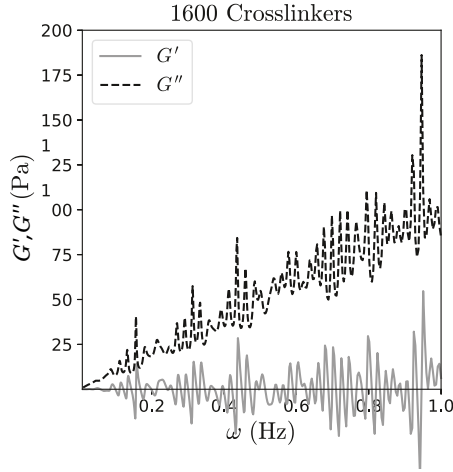


Figure 3.2: Viscous (G'') and Elastic (G') moduli extracted from bead MSD.

The MSD and the complex shear moduli obtained from a traditional bead microrheology-like approach indicate that it might not capture the viscoelastic properties of the network. Further examination of this system (in Appendix Sec. B.1) suggests that this might result from inherent limitations in Cytosim as opposed to a sub-optimal choice of system parameters.

3.3 Segment Tracking Microrheology

Following the limitations of bead microrheology (Sec. B.1), we switched to segment tracking microrheology (STM), a method proposed by Kim *et al.* [17] to probe cytoskeletal networks using filament segments. Unlike inert beads, segments are embedded within the network and reflect its intrinsic mechanical properties, offering a more direct measure of

viscoelasticity.

3.3.1 Using Segments as Probes

Since filament segments, unlike beads, also have additional constraints and do not demonstrate diffusive behaviour, we tracked segments of free filaments and calculated G^* , characterizing its viscoelastic behaviour (Fig. 3.3).

Both the elastic and viscous moduli follow a power law of $G \propto \omega^{3/4}$, consistent with experimental observations [25]. While the filament segments do show inherent elasticity, they are still largely viscous. Furthermore, at the lower end of the frequency regime, the elastic modulus is 1-2 orders of magnitude smaller than the plateau value of G' observe in cross-linked networks (Fig. 3.8). Therefore, we can be certain that the observed viscoelastic properties arise from the network and not due to the constrained dynamics of the probe.

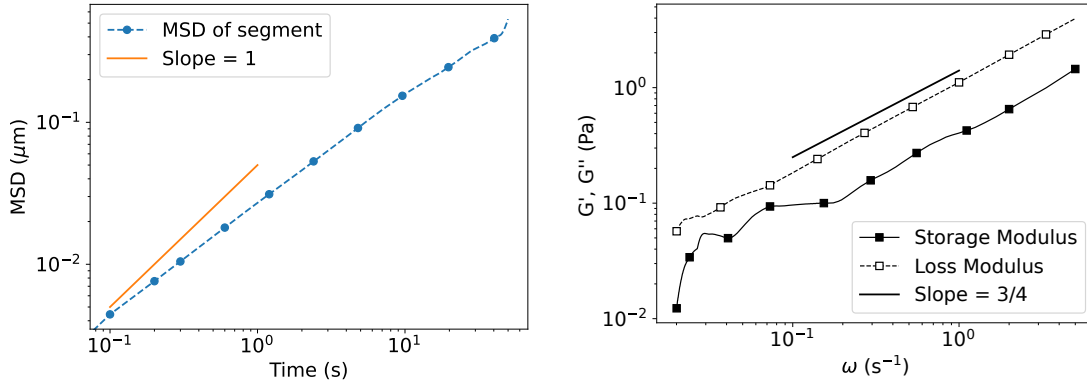


Figure 3.3: MSD and Shear Modulus for a free filament segment

3.3.2 Tracking Segments and Modification

Unlike beads, the MSD of segments in the cross-linked network does show subdiffusive behaviour (Fig. 3.4 (Left)). It was also observed that increasing the cross-linker concentration had a substantial effect on the MSD, as expected from literature.

Calculating G^* (Fig. 3.4 (Right)) shows that the system is viscoelastic, showing elastic behaviour at low frequencies and viscous behaviour at higher frequencies. This qualitatively matches the results obtained by Kim *et al.* [17]. However, quantitatively, it was observed that the crossover from elasticity-dominated to viscosity-dominated regimes occurred at a frequency of ≈ 0.1 Hz, an order of magnitude lower than the frequency at which Kim *et al.* [17] observed the crossover.

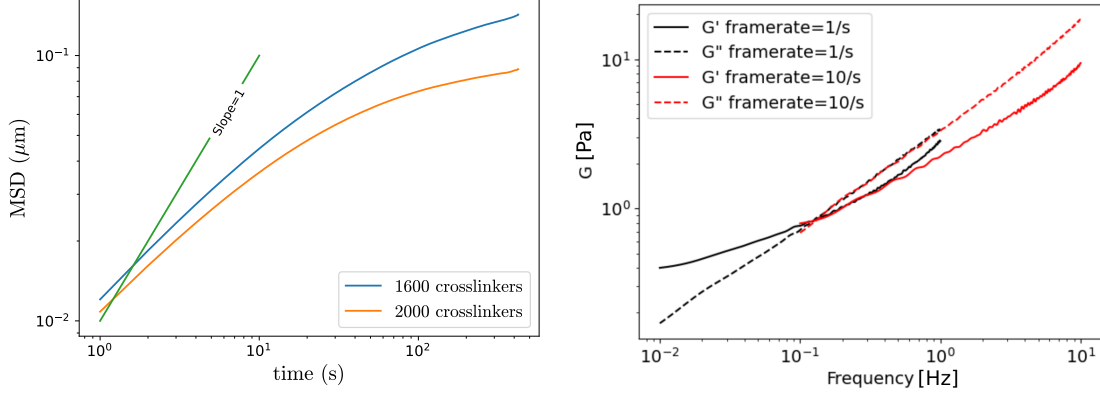


Figure 3.4: (Left) Mean Squared Displacement (MSD) of filament segments for two different cross-linker counts. (Right) Storage and loss moduli G' and G'' for the system with 1600 cross-linkers. The red and black plots correspond to simulations of different durations, sampled at different framerates.

3.3.3 Matching benchmark simulation

The observed crossover frequency mismatch with Kim *et al.* [17] likely arises from differences in simulation parameters. While we were able to adapt almost all parameters from the benchmark simulation into Cytosim, some parameter values were simply not specified in the Kim *et al.* publication. In particular, the viscosity of the medium in the benchmark simulation was unknown, resulting in the usage of Cytosim's default viscosity of $\eta = 0.1 \text{ Pa} \cdot \text{s}$ (roughly 1000-times the viscosity of water emulating the intra-cell environment).

Effect of Viscosity

To explore how changing medium viscosity might affect the crossover in simpler systems, consider a non-Newtonian fluid described by the Maxwell model (Sec. 1.2.1). From Eq. 1.5 we have,

$$G'(\omega) = \frac{G\eta^2\omega^2}{\eta^2\omega^2 + G^2} \quad (3.1)$$

$$G''(\omega) = \frac{G^2\eta\omega}{\eta^2\omega^2 + G^2} \quad (3.2)$$

The crossover point ω_0 where $G'(\omega_0) = G''(\omega_0)$ is then given by,

$$\frac{G\eta^2\omega_0^2}{G^2\eta\omega_0} = \frac{G'(\omega)}{G''(\omega)} = 1$$

$$\omega_0 = \frac{G}{\eta} \quad (3.3)$$

$$\ln \omega_0 = \ln G - \ln \eta \quad (3.4)$$

Eq. 3.4 demonstrates that, for a Maxwell solid, an increase in viscosity shifts the crossover point to the left. More generally, since the ‘characteristic timescale’ for a viscoelastic material (over which the material stores energy) is given by $\tau = \eta/G$ (Sec. 1.2.1); the larger the medium viscosity, the longer the elastic modulus dominates i.e. the crossover happens at smaller frequencies.

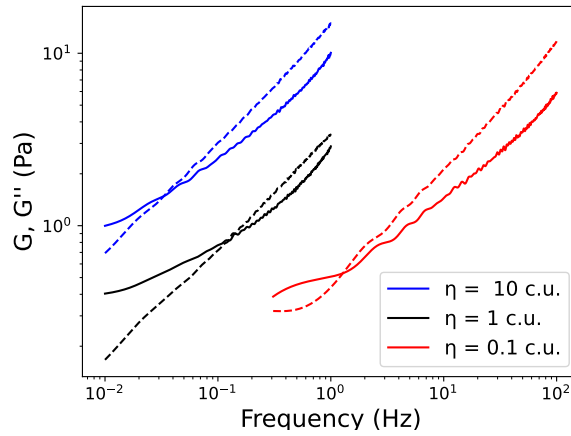


Figure 3.5: A decrease in the medium viscosity shifts the crossover to the right. The viscosity η is represented in Cytosim Units ($\text{pNs}/\mu\text{m}^2$), where 1 c.u. is approximately 1000 times the viscosity of water.

This matches with our observations on changing the viscosity of the medium. Moreover, we noticed that using a viscosity 100 times that of water, the shear moduli were in good agreement (with a maximum deviation of 18% for G' and 15% for G'') with the benchmark simulation. Fig. 3.6 shows a comparison between the results of our simulations and the reference.

While we do not obtain a perfect match, there are other fundamental differences between our system and the reference simulation (for example, the cross-linkers modelled by Kim *et al.* [17] have a fixed resting length and additional bending rigidities) which might explain slight discrepancies between the two simulations.

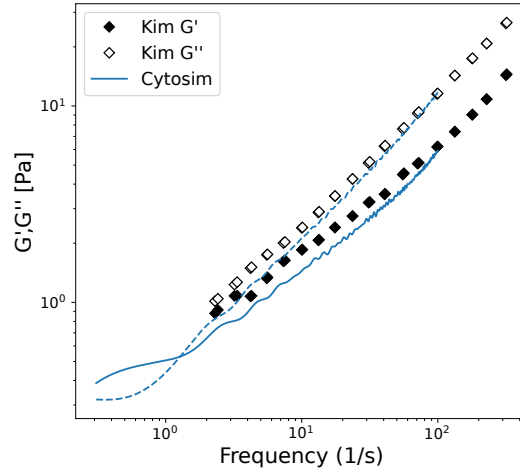


Figure 3.6: Comparison of our results G^* with the benchmark. The storage (\blacklozenge) and loss (\diamond) moduli are of the same order of magnitude across the frequency range. The data points for the reference simulation were extracted from Kim *et al.* [17] (2009) using Engauge Digitizer.

3.4 Parameter scans

Having tested and validated our setup, we studied the effect of increasing cross-linker concentration in the system varying the number of cross-linkers from 0 to 9000 in regular steps. From literature [24], we expect the network to become more elastic/solid-like with increasing cross-linker concentrations.

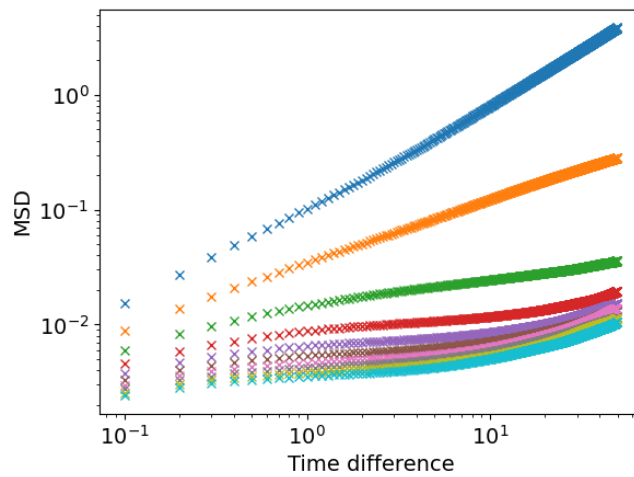


Figure 3.7: MSD: Varying Cross-linker Concentrations

Segment MSDs (Fig. 3.7) suggest a transition from diffusive to subdiffusive (potentially viscoelastic) behaviour with increasing cross-linker counts.

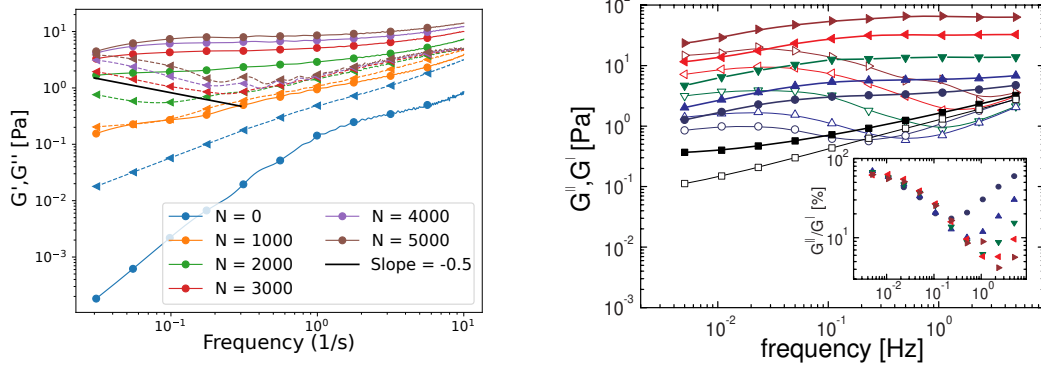


Figure 3.8: (Left) Frequency dependent G^* for increasing cross-linker concentrations. Irrespective of the number of cross linkers, at the loss moduli converge to a high-frequency power law of $G'' \propto \omega^{0.75}$. (Right) Experimental result from Tharmann *et al.* [26], showing G' (storage modulus) and G'' (loss modulus) in a system with increasing concentration of crosslinkers ($\square = 0.02\mu M$, $\circ = 0.14\mu M$, $\triangle = 0.29\mu M$, $\nabla = 0.73\mu M$, $\triangleleft = 1.35\mu M$, $\triangleright = 2.71\mu M$.) Around $\omega = 0.1$, both experiment and simulation show a plateau in G' and a power law of $\omega^{-0.5}$ for G'' in systems with high crosslinker concentrations

The complex shear moduli obtained from our simulations have been plotted in Fig. 3.8 (Left), omitting cross-linker counts over 5000 for clarity. Appendix Fig. D.1 shows the elastic and viscous shear moduli across the full range of cross-linker concentrations, which follow a similar trend. Shown on the right are results from similar *in vitro* experiments conducted by Tharmann *et al.* [26].

In line with theoretical expectations, we observe an increase in both the elastic modulus and the magnitude of the complex shear modulus ($|G^*|$) with increasing cross-linker concentration (Fig. 3.9).

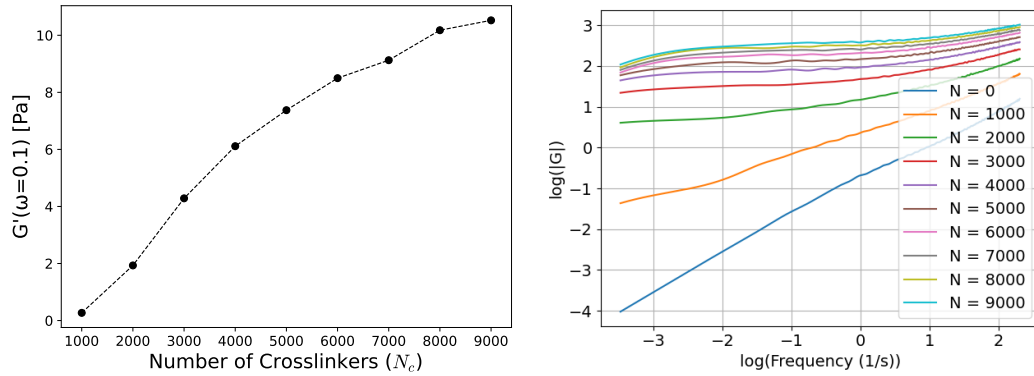


Figure 3.9: (Left) Value of G' at frequency $\omega \approx 0.1$. For $N_c \geq 3000$, this lies in the plateau for G' . (Right) Absolute value of frequency dependent G^* for different value of N_c .

The results are also in qualitative agreement with the experimental work by Tharmann *et al.* [26] involving Actin networks cross-linked with Heavy Meromyosins (HMMs), showing trends and similar power law behaviour.

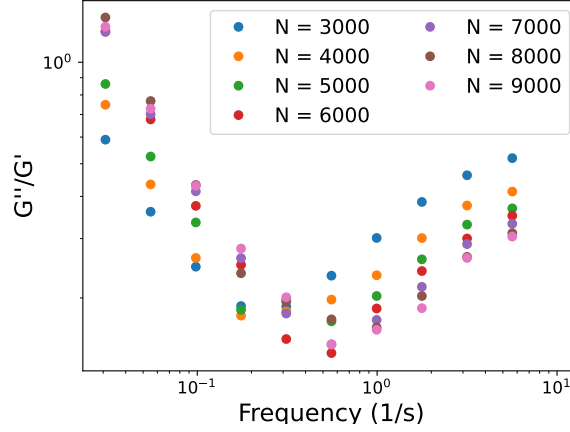


Figure 3.10: Creep (G''/G') vs ω

We also observe an increase in the creep (G''/G') at lower frequencies (Fig. 3.10, Fig. 3.8 (Right, inset)).

From Fig. 3.7, it can be seen that in the absence of cross-linkers, the system displays (close to) purely viscous behaviour, in agreement with literature [27].

The plateau value of the storage modulus increases with increasing cross-linker concentrations (Fig. 3.9). We also observe a slight decrease in G' at lower frequencies.

Comparison with Experiments

To validate our results, we compared it against experimental work by Tharmann *et al.* [26], which looks at the effect of increasing cross-linker concentrations in *in vitro* reconstituted actin networks cross-linked by heavy meromyosin (HMM). Their choice of cross-linker is of particular interest to us, since HMM has a very high binding affinity for actin (about four orders of magnitude higher than the cellular cross-linker α -actinin). As a result, the changes in rheology of the network is not dominated by unbinding of cross-linkers, but rather by folding/unfolding of filaments. Since we use cross-linkers that never unbind, we expect their observations to better represent our system. However, it has to be noted that, unlike in our setup, the cross-linkers used by Tharmann *et al.* [26] *can* unbind at sufficiently high forces. Furthermore, the experimentalists measured rheology using a Rheometer (Sec. 1.2.3), and as a result, could sample much lower frequencies.

Qualitatively, our system manages to capture several features reported by Tharmann *et al.* Both the experimental work and our simulations show a frequency regime where the viscos-

ity modulus follows a power law of -0.5 ($G'' \propto \omega^{-0.5}$) followed by an increase (Fig. 3.8) with the minima roughly corresponding to region where G' approaches a plateau.

The Tube Model

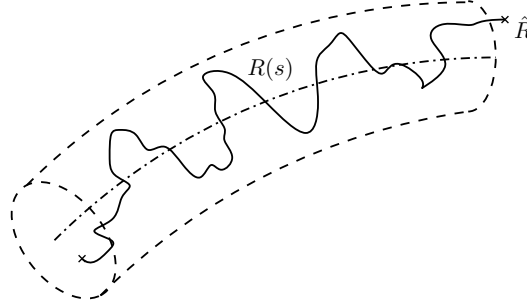


Figure 3.11: The tube model for cross-linked filament. Figure adapted from F.C. Edwards, 1988.

F. C. Edwards (1988) proposed a ‘tube’ model for cross-linked networks of rubber. In this model, the polymer section between two cross-linkers is constrained to a tube. Higher modes of vibration result from fluctuations of the segments. Therefore, the model predicts a high frequency power law of $\omega^{0.75}$ (which our measurements in Sec. 3.3.1 capture via the fluctuations of the filament segments). This theory also predicts an intermediate frequency power law of $\omega^{-0.5}$ for the loss modulus due to the constrained motion. For even smaller frequencies, one would expect diffusive behaviour (according to the tube model), but our current simulations are not long enough to sample this.

3.5 Introducing Renewal

While the previous simulations assumed a constant length for simplicity, in the cell actin filaments undergo turnover and depolymerization [21] which might have a significant effect on the rheology of the system. In order to explore this further, we introduced the following models of renewal of actin into our system.

3.5.1 Cut and Paste Renewal

As a first test, we adopted a very simple model for renewal of filaments proposed by Belmonte *et al.* [18], where a random filament is deleted and added back at a different position (Sec. 2.3.1). We added 50 probe filaments to obtain MSDs that span the entire duration of the simulation.

Fig. 3.12 (a) shows the MSDs for different rates of renewal (r_{new}). For higher rates of renewal, it was seen that the probe filaments form bunches (Fig. 3.12 (b,c)). This suggests

that the anomalous behaviour of the MSD at higher renewal rates might be an artefact. Interestingly, we observe a considerable difference in the MSD at $r_{new} = 0.25s^{-1}$, where only 12 of the 550 filaments have a chance to undergo renewal.

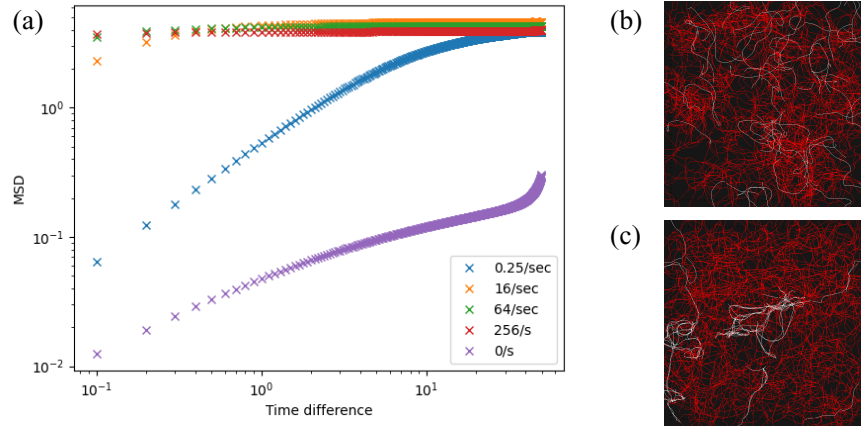


Figure 3.12: (a) MSD of probe filaments (b) Snapshot of simulation with $r_{new} = 0.25s^{-1}$ (c) Snapshot of simulation with $r_{new} = 256s^{-1}$: Non renewing (probe) filaments are shown in white

The bunching up of probe filaments has a straightforward explanation—In the CnP renewal scheme, a filament loses its cross-links upon deletion, freeing up cross-linkers in that process. These cross-linkers can bind to other filaments. However, since probe filaments never renew, the number of cross-linkers bound keeps increasing. Eventually, most cross-linkers are bound to the non-renewing filaments, leading to the formation of bunches.

This demonstrates a major limitation of STM. Since the probes in STM are a part of the network (rather than the inert probes in bead microrheology), there is little to no guarantee that heterogeneous probes will be capable of measuring the viscoelastic properties of a system. This would also be an important consideration for systems with multiple kinds of filaments.

To eliminate issues with heterogeneous probe filaments, it is necessary to conceive a mode of renewal where the all filaments also undergo identical renewal, while also ensuring that a sufficient number of segments can be tracked over the total duration of the simulation.

3.5.2 Run and Tumble (RnT) renewal

The more realistic RnT technique presented in Sec 2.3.2 does not have this problem since all filaments are identical, and there are no direct deletion events.

We implemented the length dependent (LDR) renewal strategy described in Sec. 2.3.2 to overcome the issue of the changing filament length distributions. Simulations were then run

with the following switching rates:

$$r_{g \rightarrow s} = \begin{cases} 0.4 \text{ s}^{-1} & l > 1.6, \\ 0 \text{ s}^{-1} & \text{otherwise} \end{cases} \quad r_{s \rightarrow g} = \begin{cases} 0.4 \text{ s}^{-1} & l < 1.4, \\ 0 \text{ s}^{-1} & \text{otherwise} \end{cases} \quad (3.5)$$

where $r_{g \rightarrow s}$ and $r_{s \rightarrow g}$ are the rates at which a filament of length l changes from growing to shrinking and vice versa.

Fig. 3.13 shows snapshots of network length distribution ϕ_L at different times in the simulation where filaments undergo RnT renewal with (b) and without (a) length dependent renewal (LDR), demonstrating that LDR is capable of maintaining a constant ϕ_L for the entire duration of the simulation.

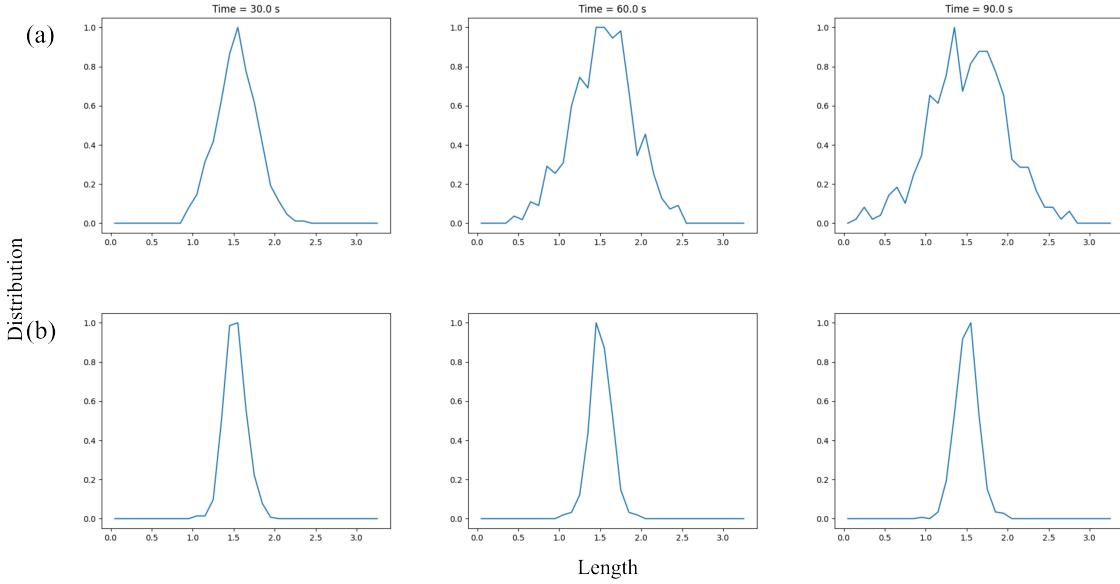


Figure 3.13: Filament length distribution as a function of time (a) Uniform Switching Rates (b) Length Dependent Switching rates: The y-axis has been normalized to $[0,1]$. With uniform switching rates, the length of filaments increases with time, while LDR maintains a steady-state distribution.

To study the effect of the RnT renewal model, we simulated a system with parameters identical to the ones in Sec. 3.3.3, and allowed the filaments to grow and shrink. Additionally, to act as control for renewal, another simulation was run where filament growth/shrinkage was switched off after reaching the steady-state length distribution, creating a non renewing system with the same length distribution as the renewing system (Wider Length Distribution, Fig. 3.14). For comparison, the MSD of the system from Sec. 3.3.3 has also been plotted in Fig. 3.14.

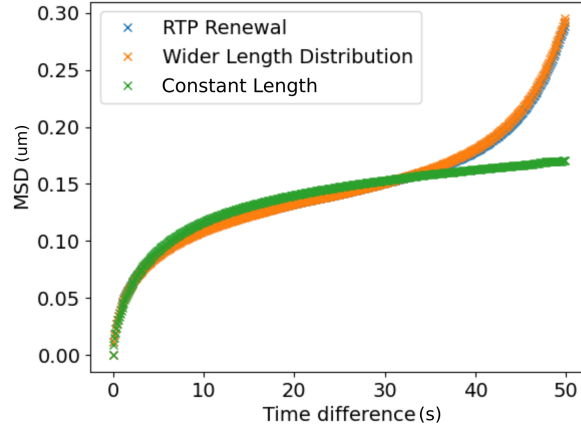


Figure 3.14: Segment MSD for filaments undergoing RnT renewal, compared against non-renewing filaments. The orange curve, where renewal was stopped after equilibration, is identical to the blue curve (with renewal). However, both the curves differ from the case where all filaments in the network have an identical length

Results show that while the MSD is different for the renewing case, it does not change if the renewal is stopped after equilibration. This suggests that, in the case of RnT renewal as described in Sec. 2.3.2 the change in the MSD is caused by the altered length distribution rather than renewal itself.

Is there *really* Renewal?

While LDR works well in conjunction with STM, there are a few caveats that might be responsible for the apparent effect (or the lack thereof) of introducing renewal. For example, with the chosen parameters, the filament length distribution (shown in Fig. 3.13 (b)) has a standard deviation of $0.13\mu\text{m}$ (a length decrease of $\sim 0.06\mu\text{m}$).

A rough estimate for the fraction of fully and partially unbinding cross-linkers (see Sec. A.3) gives:

$$\begin{aligned}\phi_{\text{Partial}} &= \frac{1}{l_0} \frac{\sigma}{\sqrt{2\pi}} \approx 0.03 \\ \phi_{\text{Full}} &= \frac{1}{4l_0^2} \frac{\sigma^2}{\pi} \approx 0.005\end{aligned}\tag{3.6}$$

With sufficient renewal, we expect changes in the viscoelastic behaviour resulting from transient network reorganization caused by binding and unbinding of cross-linkers. However, Eq. 3.6 indicates that LDR triggers very few cross-linker unbinding events, resulting in negligible structural changes.

We have shown that, with this model, renewal does not lead to significant differences. However, Fig. 3.5.2 does show that a change in the MSD can arise from a non-degenerate length distribution (Blue and Orange curves vs the green control). From Sec. 2.2.4, we know that the mobility (and hence MSD) of a filament depends on its length. To check if this can explain the deviation, let us consider a single filament of length l with the mobility μ showing subdiffusive behaviour. The MSD would be of the form

$$\langle r^2 \rangle \propto \mu t^\alpha \quad \alpha < 1$$

Since μ is inversely proportional to l ,

$$\langle r^2 \rangle \propto \frac{t^\alpha}{l} = \kappa \frac{t^\alpha}{l} \quad (3.7)$$

For an arbitrary length distribution $\phi(l)$, the average MSD is give by

$$\begin{aligned} \langle \langle r^2 \rangle_t \rangle_l &= \int_0^\infty \psi(l) \langle r^2 \rangle(l) dl \\ &= \int_0^\infty \psi(l) \kappa \frac{t^\alpha}{l} dl \end{aligned} \quad (3.8)$$

From Eqn. 3.8, it is evident that changes in mobility alone cannot affect power law behaviours of the MSD. Moreover, if the length distribution is a narrow symmetric function (as in the case of LDR) centered around l_0 , we can compute the integral, obtaining an expression for the ensemble MSD:

$$\begin{aligned} \langle \langle r^2 \rangle_t \rangle_l &= \int_{-\infty}^\infty \psi(\Delta l) \kappa \frac{t^\alpha}{l_0 + \Delta l} d\Delta l \\ &= \int_{-\infty}^\infty \psi(\Delta l) \kappa \frac{t^\alpha (1 - l/l_0)}{l_0} d\Delta l \quad (\Delta l \ll l_0) \\ &= \int_{-\infty}^\infty \psi(\Delta l) \kappa \frac{t^\alpha}{l_0} d\Delta l - \int_{-\infty}^\infty \psi(\Delta l) \kappa \frac{t^\alpha l}{l_0^2} d\Delta l \quad \xrightarrow{0 \text{ (Odd Function)}} \\ &= \kappa \frac{t^\alpha}{l_0} = \langle r^2 \rangle(l_0) \end{aligned} \quad (3.9)$$

Clearly, the deviation in the MSD from the control is not an obvious effect of introducing a wider length distribution. This suggests that the length distribution plays a role in the overall network structure, revealing interesting physical behaviour.

3.6 Cytocalc

To facilitate reproducible analysis of Cytosim simulations and extract viscoelastic properties, we developed Cytocalc, an open-source Python package. Cytocalc aims to address the lack of standardized tools for analyzing Cytosim simulation outputs by providing robust parsers for Cytosim’s (various) report files and convenience functions for interfacing with other popular analysis packages, such as Freud.

Through a straightforward API, Cytocalc offers tested and fast implementations of Evans’ and Mason’s methods. While currently tuned for rheology measurements, the parser functionality of Cytocalc allows it to form the basis for a more general-purpose Cytosim analysis package. Furthermore, the open-source nature of Cytocalc ensures that the code is modifiable and easily accessible, promoting collaboration.

Chapter 4

Conclusion

4.1 Summary

In this masters' thesis, we systematically investigated the viscoelastic properties of cross-linked actin networks using Cytosim, showing that it is possible to capture the viscoelastic behavior of cytoskeletal networks using segment tracking microrheology (STM).

The traditional bead-based approach failed to capture network viscoelasticity, likely due to inherent constraints in modeling bead-network interactions within Cytosim. Filament segments, on the other hand, proved to be effective as probes for microrheology, revealing sub-diffusive dynamics and frequency-dependent shear moduli (G' , G'') consistent with known power-law behaviors (e.g. $G'' \sim \omega^{-0.5}$ at intermediate frequencies and $G \sim \omega^{0.75}$ at high frequencies). Parameter scans of cross-linker concentrations mirrored experimental trends, showing increased elasticity and $|G^*|$ with cross-linker density. Comparing the power laws with predictions from the tube model for cross-linked networks in rubber showed that the timescale of the simulations was comparable to the Rouse time τ_R .

In order to test the effects of renewal, two strategies—Cut-and-Paste (CnP) and Run-and-Tumble (RnT)—were explored. While CnP renewal introduced artifacts due to heterogeneous probe filaments at high rates of turnover, significant changes in the mean-squared displacement (MSD) was observed even at lower rates.

With RnT renewal, it was demonstrated that usign length-dependent regulation (LDR) can profuce stable filament distributions. However, cross-linker unbinding events were limited under tested parameters, resulting in minimal restructuring of the network. As a consequence, the effect of renewal on the physical properties was minimal. This foray into RnP renewal also suggested that the distribution of lengths might play a role in the viscoelastic properties.

With the aim of facilitating the use of Cytosim for viscoelastic measurements, a Python package, *cytoalc*, was developed to perform rheological analysis on Cytosim outputs, enabling robust extraction of $G^*(\omega)$ via Evans' and Mason's methods.

4.2 Outlook

Having shown that Cytosim can be employed as a tool for probing the rheology of network, the focus on future efforts would be to improve and refine the protocols proposed herein.

4.2.1 Quantitative Matches with Experimental Results

In this thesis, it was shown that STM in Cytosim can produce quantitative matches with simulations from literature. We also presented a qualitative comparison to experimental results. In collaboration with experimental groups, further validation of the approach can be established by matching the results quantitatively by mimicking the setup as closely as possible.

4.2.2 Rheology Techniques

The work presented in this thesis largely involved testing and characterizing results from passive microrheology. Notably, the bead probe had to be replaced by segments to accurately capture the elastic properties. However, as seen with the results of CnP renewal, segments being a part of the network creates additional requirements on the probe.

Apart from passive microrheology, other local techniques like active bead microrheology and two-point microrheology can also be employed to extract the complex shear modulus. It is yet to be explored if one of these techniques work with inert beads, which would allow for straightforward measurements on compound, dynamic and active networks.

Moreover, using the virial pressure of the system as a proxy for stress, it might be possible to emulate bulk rheology techniques in Cytosim. Since the frequency of the applied shear strain can be tuned, this would also allow probing larger frequencies than what can be studied with microrheology, where the timestep and duration of the simulation present inherent limitations (Appendix Sec. B.2).

4.2.3 Renewal Models

Since the preliminary renewal models used had several limitations, there is a need for development of biophysically accurate renewal mechanisms that better mimic actin treadmilling or motor-driven turnover. Aligned with this goal would be efforts to match typical length dis-

tributions of actin inside the cell. Incorporating force-dependent unbinding rates for cross-linkers might also facilitate network remodeling in living cells.

4.2.4 Activity and Network Complexity

With an established protocol, characterization of more complex systems becomes viable. Contractile actin networks with molecular motors can be used to study how active stresses modulate viscoelasticity. Similarly, compound networks of Actin and Intermediate filaments can lead to rich physical responses. Studying these would require refinements to our current technique, especially regarding the choice of probes.

Ultimately, the ease of simulation complex systems in Cytosim and having a framework for probing the rheology thereof offer several venues for future research involving semiflexible networks.

Appendices

Appendix A

Derivations

A.1 The Generalized Stokes Einstein Relation

In this section, we present the derivation for a Generalized Stokes-Einstein Relation (GSER) provided by Mason *et al.* [14]. A passive Brownian particle moving in a viscous medium is well described by the Langevin equation

$$m\dot{v}(t) = f_S(t) - \gamma v(t)dt \quad (\text{A.1})$$

For a particle in a non-newtonian fluid, Zwanzig *et al.* [28] proposed an analogous drag coefficient that depends not only on the particle's current velocity but also on its history. Using this in Eq. A.1 gives us the generalized langevin equation [15]:

$$m\dot{v}(t) = f_S(t) - \int_0^t \zeta(t-t')v(t')dt' \quad (\text{A.2})$$

For a purely viscous case, the function $\zeta(t-t')$ is simply $\gamma\delta(t-t')$. Applying a unilateral Fourier transform on Eq. A.2, we get:

$$\tilde{v}(\omega) = \frac{mv(0) + \tilde{f}_S(\omega)}{im\omega + \tilde{\zeta}(\omega)} \quad (\text{A.3})$$

For an overdamped system, the inertia component $m\omega$ is significantly smaller than the drag component; hence, we can neglect the term in the denominator:

$$\tilde{v}(\omega) = \frac{mv(0) + \tilde{f}_S(\omega)}{\tilde{\zeta}(\omega)} \quad (\text{A.4})$$

To obtain the velocity autocorrelation function, we multiply Eq. A.4 by $v(0)$ and take the average on both sides:

$$\langle v(0)\tilde{v}(\omega) \rangle = \frac{m\langle v^2(0) \rangle + \langle v(0)\tilde{f}_S(\omega) \rangle}{\tilde{\zeta}(\omega)} \quad (\text{A.5})$$

Using Equipartition theorem $m\langle v^2(0) \rangle = 3k_B T$ and recognizing that the stochastic force f_S and v are uncorrelated,

$$\langle v(0)\tilde{v}(\omega) \rangle = \frac{3k_B T}{\tilde{\zeta}(\omega)} \quad (\text{A.6})$$

Since the velocity autocorrelation function is related to the MSD as follows:

$$\langle v(0)\tilde{v}(\omega) \rangle = \frac{-\omega^2}{2} \langle \Delta \tilde{r}^2(\omega) \rangle \quad (\text{A.7})$$

we get,

$$\langle \Delta \tilde{r}^2(\omega) \rangle = -\frac{6k_B T}{\zeta(\omega)\omega^2} \quad (\text{A.8})$$

Assuming that Stokes' law works similarly for the frequency dependent drag coefficient, we have $\zeta(\omega) = 6\pi\eta^*(\omega)a$, which upon being substituted into Eq. A.8 gives us the GSER.

$$\langle \Delta \tilde{r}^2(\omega) \rangle = -\frac{k_B T}{\pi\eta^*(\omega)\omega^2 a} \quad (\text{A.9})$$

A.2 Crosslinker Binding Time

Each 'hand' of a cross-linker binds at a rate of κ_b (binding rate = 10s^{-1}) if it is within a distance r_b (binding range = $0.002\mu\text{m}$) of a filament. Therefore, the effective binding rate for a cross-linker, k , is given by:

$$k = P_b \cdot \kappa_b$$

where P_b is the probability for a cross-linker to be in the binding range. We can estimate using the volume fraction of filaments, treating them as cylinders with a radius r_b . Therefore,

$$k = \kappa_b \frac{N_f L_f \pi r_b^2}{V} \quad (\text{A.10})$$

$$\begin{aligned} &= \frac{10 \times 500 \times 1.5 \times \pi \times (0.02)^2}{2.8 \times 2.8 \times 2.8} \\ &\approx 0.43 \end{aligned} \quad (\text{A.11})$$

Since the network is nearly (and ideally) isotropic, we can assume that the binding rate is identical for both free and single-bound cross-linkers. Using this, we set up the Master equation for this system. Let ϕ_f , ϕ_s and ϕ_d be the fraction of free, single-bound and double-

bound cross-linkers respectively in the system. Then,

$$\dot{\phi}_f = -k\phi_f \quad (\text{A.12})$$

$$\dot{\phi}_s = k(\phi_f - \phi_s) \quad (\text{A.13})$$

$$\dot{\phi}_d = k\phi_s \quad (\text{A.14})$$

Solving Eq. A.12 with an initial condition $\phi_f(0) = 1$ and substituting in Eq. A.13,

$$\begin{aligned} k\phi_s + \dot{\phi}_s &= k \exp(-kt) \\ \dot{\phi}_s \exp(kt) + k\phi_s \exp(kt) &= k \quad (\text{Rearranging}) \\ \frac{d}{dt} (\phi_s \exp(kt)) &= k \end{aligned}$$

Solving for ϕ_s and setting $\phi_s(0) = 0$,

$$\begin{aligned} \phi_s &= kt \exp(-kt) + C \exp(-kt) \\ &= kt \exp(-kt) \end{aligned} \quad (\text{A.15})$$

Substituting Eq. A.15 in Eq. A.14 and solving for ϕ_d ,

$$\begin{aligned} \dot{\phi}_d &= k^2 t \exp(-kt) \\ \phi_d &= \int k^2 t \exp(-kt) dt \\ &= \int s \exp(s) ds \quad (s = -kt) \\ &= -kt \exp(-kt) - \exp(-kt) + C \\ &= 1 - \exp(-kt)(1 + kt) \end{aligned} \quad (\text{A.16})$$

We have thus derived an analytical expression for the number of double-bound cross-linkers in the network. Comparing with bound cross-linkers data from Cytosim, we obtain a quantitative match. Using this, we can determine the ideal equilibration time for a given system.

A.3 Renewal-Driven Cross-linker Unbinding

In this section, we provide a rough estimate for the average number of crosslinker unbinding events that occur due to the shrinking of filaments, as in the case of renewal. We neglect higher order unbinding events (where a crosslinker unbinds, binds and unbinds again) since, for LDR, we expect such events to be rather rare (an argument supporting this is presented towards the end of this section).

Let us consider a system with N_f filaments of length l_0 and N_C cross-linkers. Suppose, as a result of renewal, the length distribution changes to a gaussian distribution with standard deviation σ . Then, the change in length of each filament Δl follows:

$$\psi(\Delta l) = \frac{1}{\sigma\sqrt{2\pi}} \exp\left(\frac{-\Delta l^2}{2\sigma^2}\right) \quad (\text{A.17})$$

The number of cross-linkers bound to a filament is given by $n = 2N_C/N_f$ (since each cross-linker has two hands). Assuming that the binding points are randomly distributed on a filament, the average number of cross-linkers bound to a region of length x is nx/l_0 .

Therefore, the number of first order cross-linker unbinding events (N_{ub}) due to the change in length distribution is given by

$$\begin{aligned} N_{ub} &= \int_0^\infty N_f \frac{n\Delta l}{l_0} \psi(\Delta l) d\Delta l \\ &= N_f \frac{n}{l_0} \frac{1}{\sigma\sqrt{2\pi}} \int_0^\infty \Delta l \exp\left(\frac{-\Delta l^2}{2\sigma^2}\right) d\Delta l \\ &= N_f \frac{n}{l_0} \frac{\sigma}{\sqrt{2\pi}} \end{aligned} \quad (\text{A.18})$$

Note that Eq. A.18 treats the unbinding of one of the hands of a cross-linkers as an ‘unbinding event’. For complete unbinding, the equation has to account for the second hand of the cross-linker lying in a shrunk segment. Thus,

$$\begin{aligned} N_{ub} &= \frac{1}{2} \int_0^\infty \int_0^\infty N_f \frac{nl l'}{l_0^2} \psi(l) \psi(l') dl' dl \\ &= \frac{1}{4} N_f \frac{n}{l_0^2} \frac{\sigma^2}{\pi} \end{aligned} \quad (\Delta l \rightarrow l) \quad (\text{A.19})$$

Using the values from our LDR simulations, we find that only $\sim 3\%$ undergo partial unbinding, with less than 10 cross-linkers fully unbinding. Since very few cross-linkers unbind in the first place, we can neglect higher order unbinding events.

Appendix B

Additional Results

B.1 Bead Microrheology

B.1.1 Bead Size

In experimental setups, the size of the bead used is atleast 6 times the mesh size of the network [29, 30]. To estimate the mesh size of the system, we extend the method employed by Belmonte *et al.* [18] to 3D. The probability of intersection for two filaments at an angle θ with each other would be

$$P(x|\theta) = \frac{L^3}{8V} \sin^2 \theta \quad (\text{B.1})$$

The total number of intersection X in a network with N filaments is therefore:

$$\begin{aligned} X &= \frac{N(N-1)}{2} \int_0^\pi P(\theta) P(x|\theta) d\theta \\ &= \frac{N(N-1)}{2} \int_0^\pi \frac{1}{\pi} \frac{L^3}{8V} \sin^2 \theta d\theta \\ &= N(N-1) \frac{L^3}{32V} \end{aligned}$$

Using a mesh size of $N/2X$ and substituting the values from the simulation, we estimate that the bead size should be atleast $\sim 0.2\mu\text{m}$. Other techniques for estimating the value of mesh size [24, 31] also produce similar ranges.

B.1.2 Sanity Checks

In order to confirm that the issue does not lie with the range of the parameter space/system parameters, we ran simulations with artifically high/low values of some of the parameters (Fig. B.1) but the results remained unaffected by large changes in the network.

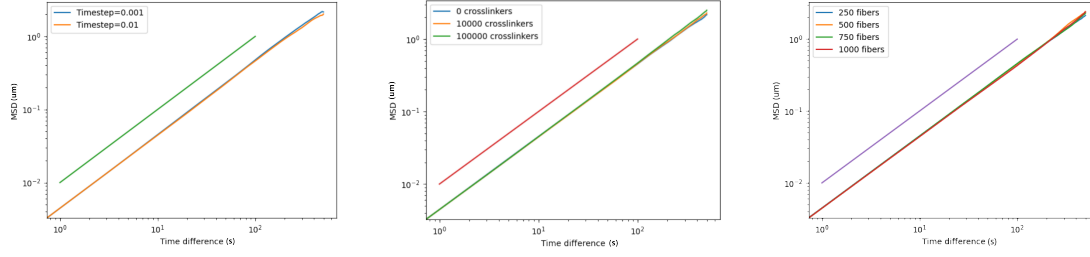


Figure B.1: MSD of bead. Testing Parameters (a) Timestep (b) Crosslinker Count (c) Actin Count

In cytosim, a bead is modelled as a point particle with a harmonic potential upto its radius R . We suspected that this might be too simplistic to capture the effect of the network.

B.1.3 Using Spheres

In addition to beads, cytosim also provides a Sphere object to represent a rigid spherical object, modelled as a bead with multiple points on its surface. Additionally, unlike the bead, the sphere is also capable of rotation. However, running simulations with the bead showed that, while the spheres did show slightly sub-diffusive behaviour, it still was unable to capture the rheology of the system. Additionally, the usage of spheres slowed the simulation down by a factor of ~ 10

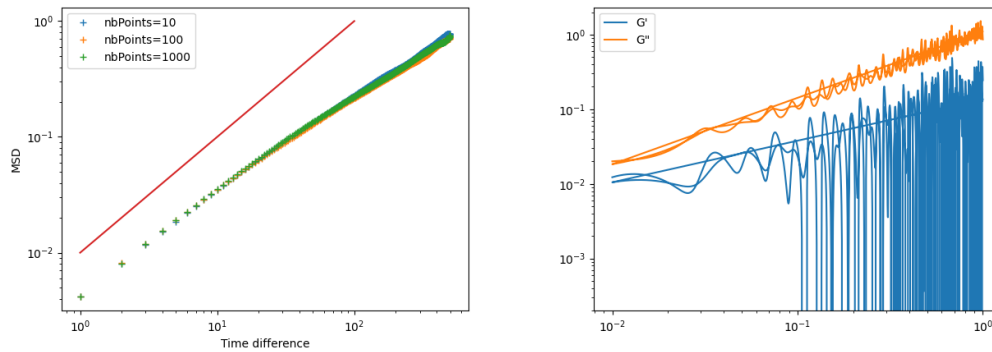


Figure B.2: (Left) MSD of Sphere. Slope of Red line = 1 (diffusive). (Right) G^* extracted from the MSD for nbPoints=1000

Fig. B.2 (Left) shows the MSD obtained from sphere (nbPoints is the number of points on the surface). While the MSD is slightly subdiffusive, the complex shear modulus does not show elasticity (Fig. B.2 (Right)). (The artifacts at higher frequencies are because of G' oscillating rapidly about 0, exacerbated by the log scale.)

B.2 Frequencies, Times and Timesteps

Since Evan’s method uses DTFT, the extracted complex shear modulus $G^* : \mathbb{R} \rightarrow \mathbb{C}$ is a continuous function of ω . However, the frequency range over which it is *valid* is limited by the frame-step (time between two ‘saved’ frames) δt_f and the total duration of the simulation T : $\omega_{\min} = 1/T$, $\omega_{\max} = 1/\delta t_f$.

As a result, gaining an additional decade in ω , requires running the simulation for 10 times as long and generating an order of magnitude more data. This is unfeasible for more than four decades, which generates over 10GB of data per simulation (including 80 ensembled). However, it is possible to run simulations of varying durations and ‘stitch’ them together, as shown in Fig.3.4 (Right). We also explored the possibility of stitching the MSDs and generating G^* from the longer MSD. This is desirable since the frame-rate can be tuned in cytosim, avoiding the need to run two separate simulations.

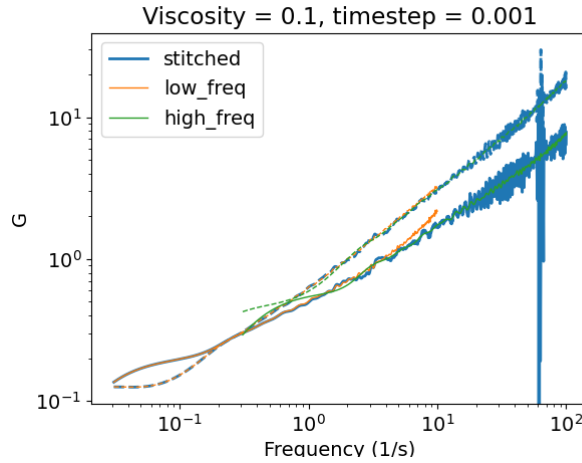


Figure B.3: G^* extracted from stitched MSD

However, with Evan’s method, the result at higher frequencies the result at higher frequencies is noisy. We suspect that this might result from the interpolation step in Evan’s method—at lower frequencies, the data is sampled solely from long-enough MSD ‘runs’. Simulations with a high-framerate, therefore, does not contribute at all to this part. However, at the high frequency regime, contributions from the linear interpolations of low-framerate data are also included. Since the linear interpolations do not contain any information about the actual high frequency fluctuations, this might explain the noisy behaviour. A DTFT scheme more resilient to non-uniform sampling (such as the Non-uniform Discrete Fourier Transform NDFT) might provide better results.

B.2.1 Timestep and Equilibration

Timestep

To prevent filaments from passing through each other, the timestep τ of the system should be small enough that distance moved by a segment (of apparent radius r) is within the steric range s_r of another segment. Assuming diffusive motion, we estimate a timestep as follows:

$$\begin{aligned}\sqrt{6\mu k_B T \tau} &\leq s_r \\ \frac{k_B T}{\pi \eta r} \tau &\leq s_r^2 \\ \tau &\leq \frac{\pi \eta r s_r^2}{k_B T} \approx 0.001 \text{ s}\end{aligned}\tag{B.2}$$

Since the motion of filaments is largely subdiffusive, we expect this to serve as a good estimate for our timestep. Running simulations with varying timesteps confirmed that the value of G' does not change significantly if timestep is lowered beyond 0.001 (Fig. B.4).

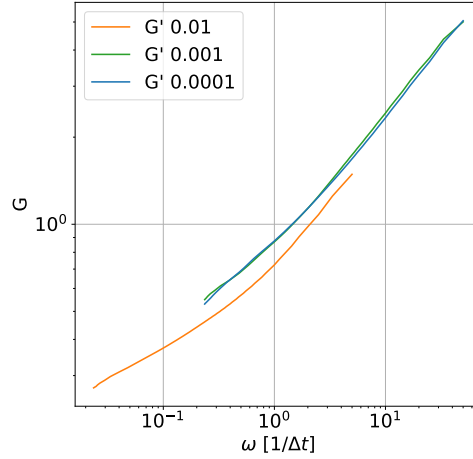


Figure B.4: Storage modulus for different timesteps

Interestingly, we observed that the loss modulus G'' varied with timestep even beyond 0.001 (Fig. D.2). This is surprising because G'' and G' can be determined from each other using the Kramers-Kronig relations [15, 32, 33].

$$G'(\omega) = \frac{1}{\pi} \int_{-\infty}^{\infty} \frac{G''(\omega')}{\omega' - \omega} d\omega' \tag{B.3}$$

$$G''(\omega) = -\frac{1}{\pi} \int_{-\infty}^{\infty} \frac{G'(\omega')}{\omega' - \omega} d\omega' \tag{B.4}$$

We suspect that these inaccuracies might arise because the algorithms we use employ a

truncated version of the Kramers-Kronig relation to compute G'' [33], however, this has to be explored further.

Equilibration

Sec. 3.4 demonstrates that the structure and properties of the network is affected greatly by the number of bound cross-linkers. Therefore, the system has to be equilibrated at least until most of the cross-linkers are bound to two filaments. An analytical estimate for the fraction of fully-bound cross-linkers (ϕ_{db}) can be obtained by writing down a Master Equation for the cross-linker hands and solving it (Appendix Sec. A.2).

$$\phi_{db} = 1 - \exp(-kt)(1 + kt) \quad (\text{B.5})$$

where k is the average binding rate of a cross-linker¹, given by

$$k = \kappa_b \frac{N_f L_f \pi r_b^2}{V} \approx 0.43 \quad (\text{B.6})$$

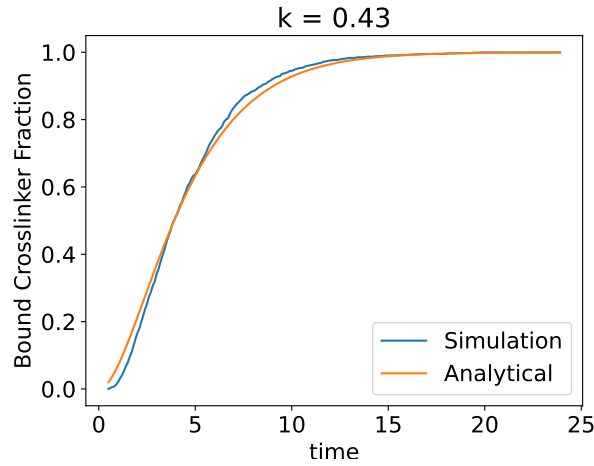


Figure B.5: Fraction of doubly bound cross-linkers vs time

From Fig. B.5, it can be seen that the analytical formula is in good agreement with the simulations. This can be used to determine a good estimate for the binding range.

¹Note that this is different from the binding rate specified in the configuration file—which is the rate given a crosslinker is within binding range of a filament

Appendix C

Technical Notes

C.1 Cytosim Configuration File

A typical configuration file for Cytosim defines the properties of the objects, the simulation duration and time step through the `set` keyword. Objects thus defined can be added to the simulation using `new`. Once the system is set up, the simulation is run for a specified number of timesteps.

```
set simul system {
    time_step = 0.001
    viscosity = 0.1
    steric = 1, 16.9, 0
}
set space cell { shape = periodic }
new cell { length = 2.8,2.8,2.8 }
set fiber actin {
    rigidity = 0.00106
    steric = 1, 0.007
    segmentation = 0.07
}
set hand binder { binding = 10, 0.02; unbinding = 0, inf }
set couple crosslinker {
    hand1 = binder; hand2 = binder
    stiffness = 4.23
    diffusion = 10
    fast_diffusion = 1
}
new 500 actin_Kim { length = 1.5 } % add filaments
run 5000 simul { solve = 1 } % Equilibration of filaments
new 1600 crosslinker % add crosslinkers
run 50000 simul { solve = 1 } % Equilibration
run 50000 simul { nb_frames = 500 } % save 500 frames
```

C.1.1 Using Templates

To facilitate the creation of config files, Cytosim provides a ‘preconfig’ script [34] that can parse blocks of python within a ‘template’ config file. This is especially useful when parameters depend on each other. For example, the file in the previous section specifies the number of timesteps for which the simulation is run. However, it is more natural to specify the total time (which also makes it robust against timestep changes). While this is not possible with a cytosim config file, we can create a template:

```
[[ timestep = 0.001 ]]
[[ duration = 50.00 ]] % in seconds
set simul system {
    timestep = [[ timestep ]]
    ...
run [[ int(duration / timestep) ]] {
```

The blocks enclosed by `[[...]]` are passed through a python interpreter. Additionally, these template files can be used to quickly generate multiple configuration files by specifying a list of numbers instead of a scalar, creating a file for each permutation.

```
[[ timestep = [0.01,0.001,0.0001] ]]
```

Syntax Highlighting

Cytosim provides a syntax-highlighting plugin for Sublime Text. vim-cytosim is a port of this plugin to Vimscript, with additional formatting features.

C.2 Reporting Random Filament Segment

With Segment Tracking Microrheology (STM), the number of probes in the system dramatically increases from 1 bead to 5000 filament segments. While having more probes does provide smoother curves, it increases computational time for an implementation of Evan’s method in python to ~5 minutes per simulation. Moreover, the report file containing trajectories of all filament segments is around 300MB in size. Using a single randomly selected segment produces equally good result, while being more efficient. It is pivotal that the choice of segment is consistent throughout the simulation. This can easily be achieved this by exploiting the deterministic property of pseudo-random numbers:

```
/* Export Fiber-number, position of random vertex per fiber */
void Simul::reportFiberRandomPoint(std::ostream& out) const
{
    out << COM << "identity" << SEP << repeatXYZ("pos") << SEP << "curvature";
    std::mt19937 rng(1);
```

```

// list fibers in the order of the inventory:
for ( Fiber const* fib = fibers.firstID(); fib; fib = fibers.nextID(fib) )
{
    out << COM << "fiber " << fib->reference()
        << " " << fib->segmentation();
    std::uniform_int_distribution<> dis(0, fib->nbPoints());
    int index = dis(rng);
    out << LIN << fib->identity();
    out << SEP << fib->posP(index);
    out << SEP << fib->curvature(index);
}
}

```

C.3 Units in Cytosim

Attached here for reference is a short list of the default units in Cytosim, as described in the Cytosim Documentation.

Parameter	Value
duration	s
length or range	um
force	pN
rate	1/s
torque	pN.um
speed	um/s
diffusion constant	um ² /s
stiffness	pN/um
angular stiffness	pN.um/rad
energy	pN.um
bending elasticity	pN.um ²
viscosity	pN.s/um ²

Table C.1: Cytosim Units

C.4 Cytosim on the Cluster

The `sim` executable, by default, lacks multi-threading capabilities. This is to encourage running it on a cluster computer, simulating each trial of the ensemble in parallel. The Institute of Theoretical Physics maintains `rocks`, a High performance Computing (HPC) unit managed by the HT-Condor queueing system.

My scripts for running cytosim simulations on the cluster are available in a public Gitlab repository: <https://gitlab.gwdg.de/vadakkeputha/cytosim-htcondor-scripts>, - along with instructions on its usage, providing a convenient way to run multiple trials for different simulations on the cluster.

Appendix D

Miscellaneous Figures

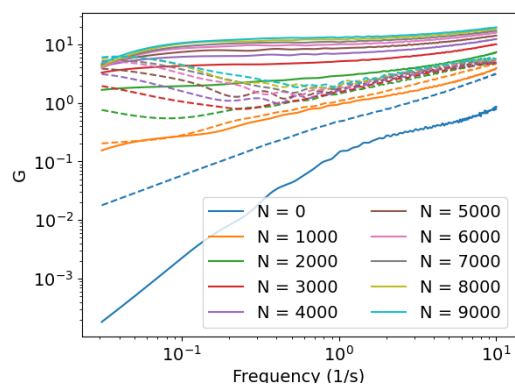


Figure D.1: Complex shear moduli with increasing number of crosslinkers.

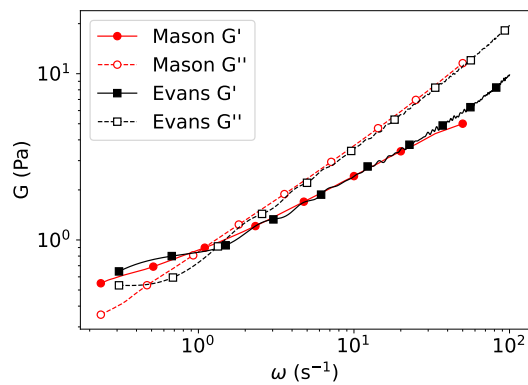


Figure D.3: Comparison: Mason's Method vs Evans' Method

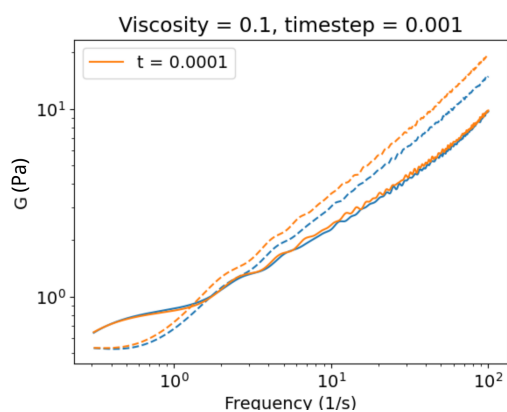


Figure D.2: Loss and Storage Moduli: Varying timesteps

Bibliography

- [1] F. Burla, Y. Mulla, B. E. Vos, A. Aufderhorst-Roberts, and G. H. Koenderink, “From mechanical resilience to active material properties in biopolymer networks,” *Nature Reviews Physics*, vol. 1, no. 4, pp. 249–263, Apr. 2019.
- [2] C. P. Broedersz and F. C. MacKintosh, “Modeling semiflexible polymer networks,” *Reviews of Modern Physics*, vol. 86, no. 3, pp. 995–1036, Jul. 24, 2014.
- [3] F. Gittes and F. C. MacKintosh, “Dynamic shear modulus of a semiflexible polymer network,” *Physical Review E*, vol. 58, no. 2, R1241–R1244, Aug. 1, 1998.
- [4] C. P. Broedersz, M. Depken, N. Y. Yao, M. R. Pollak, D. A. Weitz, and F. C. MacKintosh, “Cross-Link Governed Dynamics of Biopolymer Networks,” *Physical Review Letters*, vol. 105, no. 23, p. 238 101, Nov. 30, 2010.
- [5] J. H. Shin, M. L. Gardel, L. Mahadevan, P. Matsudaira, and D. A. Weitz, “Relating microstructure to rheology of a bundled and cross-linked F-actin network in vitro,” *Proceedings of the National Academy of Sciences of the United States of America*, vol. 101, no. 26, pp. 9636–9641, Jun. 29, 2004.
- [6] B. Hinner, M. Tempel, E. Sackmann, K. Kroy, and E. Frey, “Entanglement, Elasticity, and Viscous Relaxation of Actin Solutions,” *Physical Review Letters*, vol. 81, no. 12, pp. 2614–2617, Sep. 21, 1998.
- [7] A. G. Clark, “Chapter three - Biophysical origins of viscoelasticity during collective cell migration,” in *Viscoelasticity and Collective Cell Migration*, I. Pajic-Lijakovic and E. H. Barriga, Eds., Academic Press, Jan. 1, 2021, pp. 47–77.
- [8] J. P. Conboy, M. G. Lettinga, P. E. Boukany, F. C. MacKintosh, and G. H. Koenderink. “Actin and vimentin jointly control cell viscoelasticity and compression stiffening.” (Jan. 2, 2025), [Online]. Available: <https://www.biorxiv.org/content/10.1101/2025.01.01.630993v1> (visited on 03/21/2025), pre-published.
- [9] F. Nedelec and D. Foethke, “Collective Langevin dynamics of flexible cytoskeletal fibers,” *New Journal of Physics*, vol. 9, no. 11, p. 427, Nov. 2007.
- [10] A. C. Pipkin, *Lectures on Viscoelasticity Theory* (Applied Mathematical Sciences), F. John, J. E. Marsden, and L. Sirovich, red. New York, NY: Springer New York, 1986, vol. 7.

- [11] R. M. L. Evans, M. Tassieri, D. Auhl, and T. A. Waigh, “Direct conversion of rheological compliance measurements into storage and loss moduli,” *Physical Review E*, vol. 80, no. 1, p. 012 501, Jul. 27, 2009.
- [12] T. G. Mason and D. A. Weitz, “Optical Measurements of Frequency-Dependent Linear Viscoelastic Moduli of Complex Fluids,” *Physical Review Letters*, vol. 74, no. 7, pp. 1250–1253, Feb. 13, 1995.
- [13] V. Balakrishnan, *Elements of Nonequilibrium Statistical Mechanics*. Cham, Switzerland: Springer, 2021, 314 pp.
- [14] T. G. Mason, K. Ganesan, J. H. Van Zanten, D. Wirtz, and S. C. Kuo, “Particle Tracking Microrheology of Complex Fluids,” *Physical Review Letters*, vol. 79, no. 17, pp. 3282–3285, Oct. 27, 1997.
- [15] T. M. Squires and T. G. Mason, “Fluid Mechanics of Microrheology,” *Annual Review of Fluid Mechanics*, vol. 42, no. 1, pp. 413–438, Jan. 1, 2010.
- [16] A. V. Oppenheim, R. W. Schaffer, and J. R. Buck, *Discrete-Time Signal Processing*, 2nd ed. Upper Saddle River, N.J: Prentice Hall, 1999, 870 pp.
- [17] T. Kim, W. Hwang, H. Lee, and R. D. Kamm, “Computational Analysis of Viscoelastic Properties of Crosslinked Actin Networks,” *PLOS Computational Biology*, vol. 5, no. 7, e1000439, Jul. 17, 2009.
- [18] J. M. Belmonte, M. Leptin, and F. Nédélec, “A theory that predicts behaviors of disordered cytoskeletal networks,” *Molecular Systems Biology*, vol. 13, no. 9, p. 941, Sep. 2017.
- [19] A. Dhar, A. Kundu, S. N. Majumdar, S. Sabhapandit, and G. Schehr, “Run-and-tumble particle in one-dimensional confining potential: Steady state, relaxation and first passage properties,” *Physical Review E*, vol. 99, no. 3, p. 032 132, Mar. 26, 2019.
- [20] K. Kasza *et al.*, “Actin Filament Length Tunes Elasticity of Flexibly Cross-Linked Actin Networks,” *Biophysical Journal*, vol. 99, no. 4, pp. 1091–1100, Aug. 9, 2010.
- [21] D. S. Banerjee and S. Banerjee, “Emergence and maintenance of variable-length actin filaments in a limiting pool of building blocks,” *Biophysical Journal*, vol. 121, no. 12, pp. 2436–2448, Jun. 21, 2022.
- [22] P. C. Bressloff. “Trapping of a run-and-tumble particle in an inhomogeneous domain: The weak noise limit.” (Feb. 20, 2021), [Online]. Available: <http://arxiv.org/abs/2102.10372> (visited on 03/13/2025), pre-published.
- [23] P. Singh, S. Sabhapandit, and A. Kundu, “Run-and-tumble particle in inhomogeneous media in one dimension,” *Journal of Statistical Mechanics: Theory and Experiment*, vol. 2020, no. 8, p. 083 207, Aug. 2020.
- [24] M. L. Gardel, J. H. Shin, F. C. MacKintosh, L. Mahadevan, P. Matsudaira, and D. A. Weitz, “Elastic Behavior of Cross-Linked and Bundled Actin Networks,” *Science*, vol. 304, no. 5675, pp. 1301–1305, May 28, 2004.

- [25] F. Gittes, B. Schnurr, P. D. Olmsted, F. C. MacKintosh, and C. F. Schmidt, “Microscopic Viscoelasticity: Shear Moduli of Soft Materials Determined from Thermal Fluctuations,” *Physical Review Letters*, vol. 79, no. 17, pp. 3286–3289, Oct. 27, 1997.
- [26] R. Tharmann, M. M. A. E. Claessens, and A. R. Bausch, “Viscoelasticity of Isotropically Cross-Linked Actin Networks,” *Phys. Rev. Lett.*, vol. 98, no. 8, p. 088 103, Feb. 21, 2007.
- [27] M. Bouzid *et al.* “Transient contacts between filaments impart its elasticity to branched actin.” (Sep. 9, 2024), [Online]. Available: <http://arxiv.org/abs/2409.00549> (visited on 03/05/2025), pre-published.
- [28] R. Zwanzig and M. Bixon, “Hydrodynamic Theory of the Velocity Correlation Function,” *Physical Review A*, vol. 2, no. 5, pp. 2005–2012, Nov. 1, 1970.
- [29] S. N. Ricketts, J. L. Ross, and R. M. Robertson-Anderson, “Co-Entangled Actin - Microtubule Composites Exhibit Tunable Stiffness and Power-Law Stress Relaxation,” *Biophysical Journal*, vol. 115, no. 6, pp. 1055–1067, Sep. 18, 2018.
- [30] C. D. Chapman, K. Lee, D. Henze, D. E. Smith, and R. M. Robertson-Anderson, “Onset of Non-Continuum Effects in Microrheology of Entangled Polymer Solutions,” *Macromolecules*, vol. 47, no. 3, pp. 1181–1186, Feb. 11, 2014.
- [31] T. Golde *et al.*, “Glassy dynamics in composite biopolymer networks,” *Soft Matter*, vol. 14, no. 39, pp. 7970–7978, Oct. 10, 2018.
- [32] T. Pritz, “Unbounded complex moduli of viscoelastic materials and Kramers–Kronig relations,” *Journal of Sound and Vibration*, vol. 279, no. 3, pp. 687–697, Jan. 21, 2005.
- [33] H. C. Booij and G. P. J. M. Thoone, “Generalization of Kramers-Kronig transforms and some approximations of relations between viscoelastic quantities,” *Rheologica Acta*, vol. 21, no. 1, pp. 15–24, Jan. 1, 1982.
- [34] F. Nedelec, “Preconfig: A Versatile Configuration File Generator for Varying Parameters,” *Journal of Open Research Software*, vol. 5, no. 1, Apr. 5, 2017.
- [35] C. Das and D. J. Read, “A tube model for predicting the stress and dielectric relaxations of polydisperse linear polymers,” *Journal of Rheology*, vol. 67, no. 3, pp. 693–721, May 1, 2023.
- [36] M. Doi and S. F. Edwards, “Dynamics of concentrated polymer systems. Part 4.- Rheological properties,” *Journal of the Chemical Society, Faraday Transactions 2: Molecular and Chemical Physics*, vol. 75, no. 0, pp. 38–54, Jan. 1, 1979.
- [37] B. L. Goode, J. Eskin, and S. Shekhar, “Mechanisms of actin disassembly and turnover,” *The Journal of Cell Biology*, vol. 222, no. 12, e202309021, Nov. 10, 2023.
- [38] H. Isambert and A. C. Maggs, “Dynamics and Rheology of Actin Solutions,” *Macromolecules*, vol. 29, no. 3, pp. 1036–1040, Jan. 1, 1996.

- [39] T. G. Mason, “Estimating the viscoelastic moduli of complex fluids using the generalized Stokes–Einstein equation,” *Rheologica Acta*, vol. 39, no. 4, pp. 371–378, Aug. 1, 2000.
- [40] C. Pattamaprom, R. G. Larson, and T. J. Van Dyke, “Quantitative predictions of linear viscoelastic rheological properties of entangled polymers,” *Rheologica Acta*, vol. 39, no. 6, pp. 517–531, Nov. 1, 2000.
- [41] B. Schnurr, F. Gittes, F. C. MacKintosh, and C. F. Schmidt, “Determining Microscopic Viscoelasticity in Flexible and Semiflexible Polymer Networks from Thermal Fluctuations,” *Macromolecules*, vol. 30, no. 25, pp. 7781–7792, Dec. 1, 1997.
- [42] S. Shanbhag, “Analytical Rheology of Polymer Melts: State of the Art,” *International Scholarly Research Notices*, vol. 2012, no. 1, p. 732 176, 2012.
- [43] P. Sollich, F. Lequeux, P. Hébraud, and M. E. Cates, “Rheology of Soft Glassy Materials,” *Physical Review Letters*, vol. 78, no. 10, pp. 2020–2023, Mar. 10, 1997.
- [44] J. Xu, Y. Tseng, and D. Wirtz, “Strain Hardening of Actin Filament Networks: REGULATION BY THE DYNAMIC CROSS-LINKING PROTEIN α -ACTININ*,” *Journal of Biological Chemistry*, vol. 275, no. 46, pp. 35 886–35 892, Nov. 17, 2000.
- [45] R. M. Christensen, *Theory of Viscoelasticity: An Introduction*, 2nd ed. New York: Academic Press, 1982.
- [46] N. W. Tschoegl, *The Phenomenological Theory of Linear Viscoelastic Behavior: An Introduction*. Berlin, Heidelberg: Springer Berlin Heidelberg, 1989, 769 pp.
- [47] A. Colin *et al.*, “Recycling of the actin monomer pool limits the lifetime of network turnover,” *The EMBO journal*, vol. 42, no. 9, e112717, May 2, 2023.